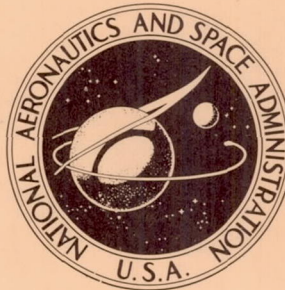


NASA TECHNICAL NOTE



NASA TN D-5156

NASA TN D-5156

**CASE FILE  
COPY**

**EXPERIMENTAL BENDING STRENGTH OF  
AN ATLAS LV-3C BOOSTER BEYOND  
COMPRESSIVE SKIN WRINKLING**

*by Robert P. Miller*

*Lewis Research Center*

*Cleveland, Ohio*

EXPERIMENTAL BENDING STRENGTH OF AN ATLAS LV-3C BOOSTER  
BEYOND COMPRESSIVE SKIN WRINKLING

By Robert P. Miller

Lewis Research Center  
Cleveland, Ohio

NATIONAL AERONAUTICS AND SPACE ADMINISTRATION

---

For sale by the Clearinghouse for Federal Scientific and Technical Information  
Springfield, Virginia 22151 - CFSTI price \$3.00

## ABSTRACT

Three bending-strength tests were performed at Lewis Research Center, on a full-scale Atlas LV-3C booster to determine the bending strength available after the start of compressive wrinkling of the vehicle tank skin. Experimental data are compared with analytical predictions and show a good correlation. A description of these tests, the test results, and a method of analytically evaluating postwrinkling bending of thin-walled pressure-stabilized cylinders are presented.

# EXPERIMENTAL BENDING STRENGTH OF AN ATLAS LV-3C BOOSTER BEYOND COMPRESSIVE SKIN WRINKLING

by Robert P. Miller  
Lewis Research Center

## SUMMARY

Three bending-strength tests were conducted on a full-scale production-type Atlas booster to satisfy three general objectives: (1) to verify the existence of postwrinkling bending strength as indicated by theory and model tests, (2) to determine the bending capability of the basic tank structure, and (3) to establish a bending-strength envelope for the entire Atlas booster.

The tests were conducted at ambient conditions with the Atlas erected in a vertical position and loaded as a beam column. Data were acquired that described the deflection-against-load characteristics of the beam, stress conditions in the tank wall, and the shape of the induced skin wrinkles.

The results of the test series indicate that the behavior of the Atlas structure under the influence of loads which induce local skin wrinkling is in reasonable agreement with theory based on beam analogy assumptions and the results of model tests. The bending load capability of the middle portion of the liquid-oxygen tank was found to be 163 percent of the wrinkling onset moment under the test conditions of internal tank pressure and axial load. The wrinkles in the tank skin remained elastic until a bending moment of approximately 150 percent of the wrinkling onset moment was applied (see fig. 24, p. 36). The third test subjected the entire Atlas booster to a bending moment loading in excess of 9 million inch-pounds ( $1.024 \times 10^6$  m-N), which qualified areas of discontinuity on the structure to sustain postwrinkling loads.

Based on the predicted moment distribution over the Atlas-Centaur for typical flights, the test results indicate that the bending strength of the entire Atlas structure is sufficient to develop the full postwrinkling moment capability ( $11.2 \times 10^6$  in.-lb or  $1.265 \times 10^6$  m-N) of the middle portion of the oxidizer tank (approx. station 800).

This report presents the test setup, results and discussion, and conclusions drawn from the series of three tests.

## INTRODUCTION

The need for lightweight structures for aerospace applications has resulted in the use of pressure-stabilized cylindrical shells for propellant tanks of large boosters. An example of such an application is the Atlas-Centaur launch vehicle (fig. 1). During the time just preceding launch and during flight, the tank structure is subjected to severe bending from aerodynamic and inertia loadings. To obtain an efficient vehicle it is essential to have a sound understanding of bending strength and mode of failure to establish a design criterion that takes full advantage of the vehicle's strength.

In the interest of defining the full bending strength inherent in pressure-stabilized structures, considerable work has been done to develop techniques for analyzing pressurized cylinders beyond the onset of compressive skin wrinkling (see refs. 1 to 4). In support of the analysis efforts, tests have been conducted to verify the analytical findings (see refs. 5 to 9). However, most of the experimental work has been performed on small (6-in. - (0.152-m-) diam) cylinders constructed of Mylar film with no circumferential joints.

While the small-scale model tests gave good correlation with the analytical findings, there remains doubt as to how well the model test results represent the behavior of cylinders of the size, type of material, and construction found in most aerospace applications. The Atlas booster, as an example, has a diameter of 120 inches (3.042 m). The skin is made of 301 extra full-hard stainless steel varying in thickness from 0.014 inch (0.000356 m) to 0.034 inch (0.000863 m). The cylinder is formed with a series of bands, approximately 30 inches (0.761 m) wide, welded together with circumferential lap joints and doubler reinforced butt-welded vertical joints (see fig. 2).

The requirement for this investigation was based on the following objections to the use of existing knowledge:

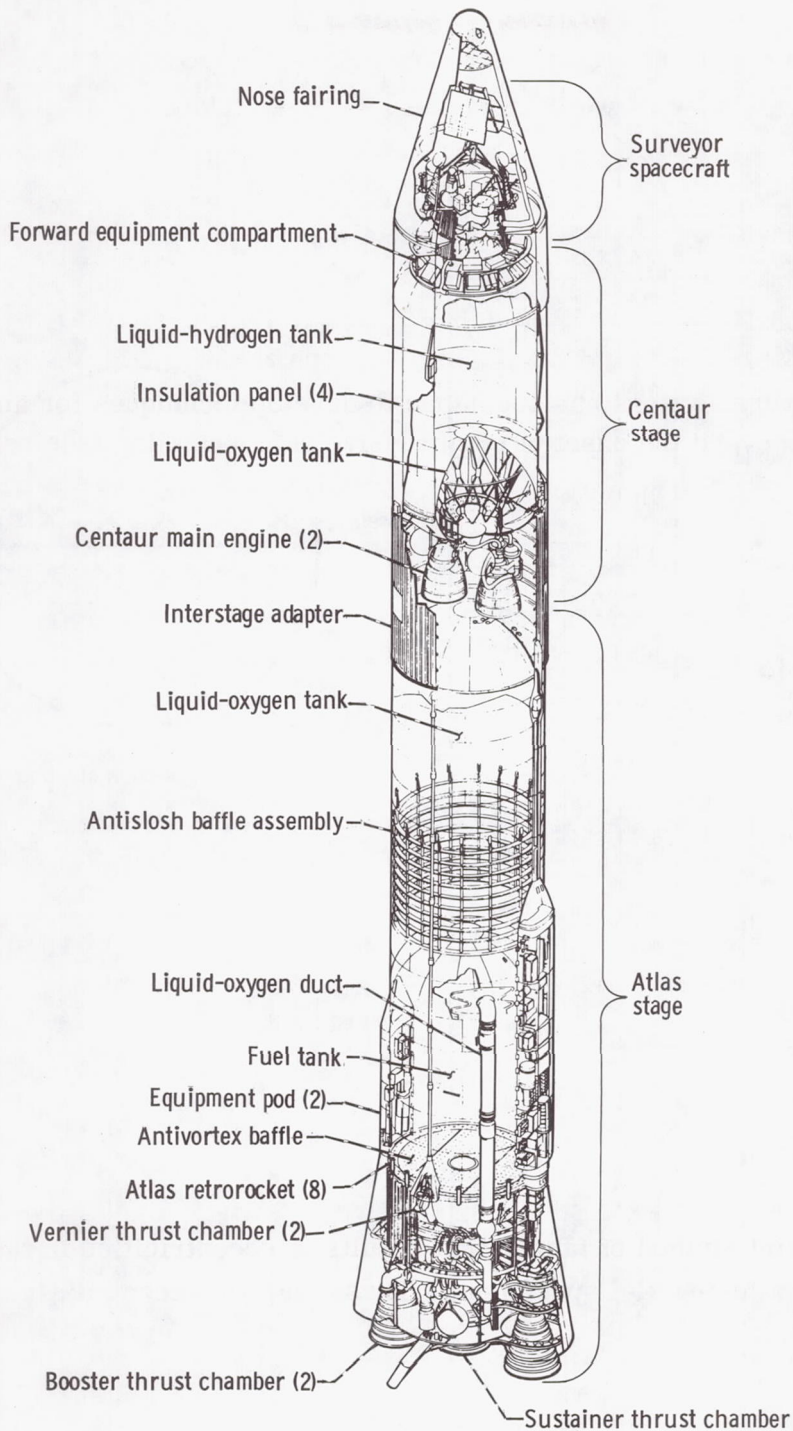
(1) The larger diameter and radius-to-thickness ratios found in the actual boosters could result in a mode of failure not exhibited by the small-scale model.

(2) The metal skin used in actual vehicles is not as elastic as the Mylar model specimens.

(3) The lap-joint method of fabrication results in eccentricities in the tank wall which are not found in the test model specimens. These built-in eccentricities could negate the predictions established by analysis and tests based on cylinders with smooth skin.

(4) The Atlas booster differs from the small specimens by having a wiring tunnel and brackets for accessories welded to the tank wall. It was essential to observe what effect these irregularities would have on the skin wrinkling pattern.

Because of these objections to a direct application of the existing knowledge of postwrinkling strength, it was decided that a thorough understanding of the bending strength of the Atlas vehicle was beyond the state of the art and that it was therefore



OC-10160-31

Figure 1. - Atlas-Centaur-Surveyor space vehicle configuration.

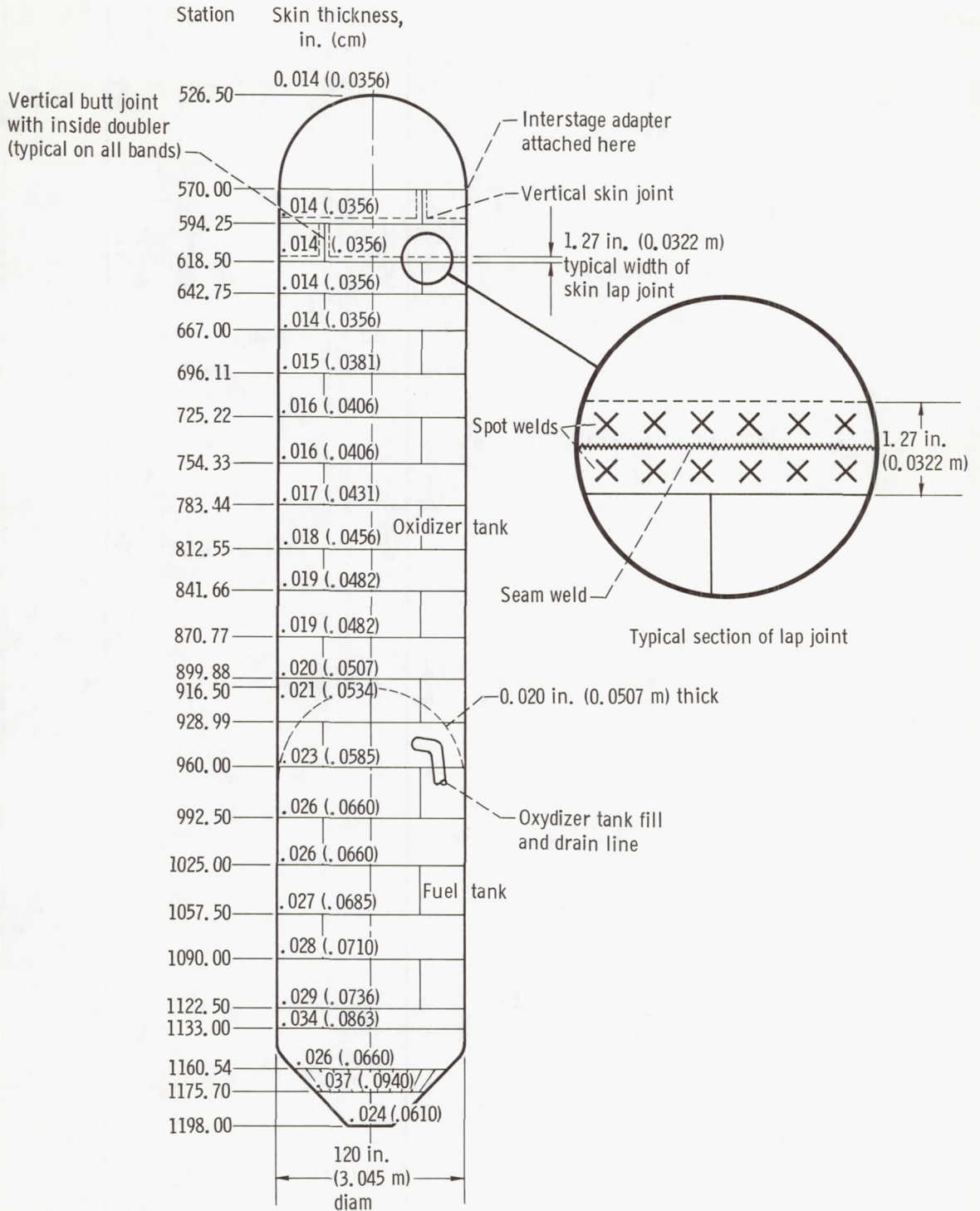


Figure 2. - Atlas test vehicle stations and propellant tank skin gages. All skins are extra full-hard 301 stainless steel.

reasonable to conduct an experimental investigation on a full-scale, production-type Atlas booster.

The investigation consisted of three tests designed to answer three specific objectives: test I was designed to verify the existence of postwrinkling bending strength in the Atlas vehicle as indicated by theory and model tests, test II was designed to determine the full bending capability of the basic tank structure, and test III was devised to establish a bending-strength envelope for the entire Atlas Booster.

The tests were carried out on a full-size Atlas LV-3C booster with the engines and their fairings removed. A flight-type interstage adapter (used to mount the Centaur second stage to the Atlas forward end) was attached to the forward end of the vehicle. The Atlas was mounted in a vertical position and loaded as a beam column with pinned ends. To simulate flight conditions, bending moment was applied simultaneously with axial load. The axial load was selected to approximate the axial loading on the Atlas during a typical Atlas-Centaur flight at the time peak bending loads are incurred (time of the maximum value of the product of angle of attack and aerodynamic pressure  $\alpha Q$ ). For all tests the propellant tanks were filled with water and pressurized to simulate flight conditions. The basic instrumentation was devised to measure strain in the tank wall, deflection of the beam, skin wrinkle shapes, and the magnitude of the applied loads.

In general, the testing followed a procedure of filling the Atlas tanks with water, establishing the specified ullage pressures, applying and holding constant the appropriate axial load, and then applying bending moment. Strain in the tank skin, deflections, and the applied loads were monitored on strip charts and recorded on magnetic tape from an analog-to-digital converter. Primary control of the loading consisted of a continuous monitoring of moment against deflection at the point of highest moment.

All of the testing described herein was performed at Lewis Research Center, Plum Brook Station, between February 1966 and August 1966.

Dr. D. J. Peery of General Dynamics/Convair was most helpful in formulating the test philosophy.

## SYMBOLS

E	modulus of elasticity, psi; $N/m^2$
$I_{\text{eff}}$	effective moment of inertia, $\text{in.}^4$ ; $m^4$
M	external bending moment, in. -lb; m-N
m	bending moment in skin in local wrinkle, (in. -lb)/in.; (m-N)/m
N	maximum load, $N_t + N_c$ , lb/in.; $N/m$

$N_c$	critical wrinkling load of skin, lb/in.; N/m
$N_t$	maximum unit tensile load, lb/in.; N/m
$N_\theta$	tensile hoop load in skin from internal pressure, lb/in. (N/m)
$P$	applied axial load, lb; N
$P_a$	external axial load, lb; N
$P_1$	axial tensile force, lb; N
$p$	internal pressure, psig; $N/m^2$ gage
$Q$	aerodynamic pressure
$R$	cylinder radius, in.; m
$R_T$	reaction to tower from shear loading
$r$	radius of curvature of centerline of elemental beam, in.; m
$r_T$	reaction to tower induced by deflections
$r_1$	radius of curvature of maximum tension fiber of elemental beam, in.; m
$r_2$	radius of curvature of maximum compression fiber of elemental beam, in.; m
$S$	applied shear load, lb; N
$\Delta S$	elemental length of cylinder, in.; m
$\delta S$	changes in elemental length of cylinder, in.; m
$t$	cylinder wall (skin) thickness, in.; m
$W$	vehicle weight, lb; kg
$w$	points where vehicle weight is considered to be concentrated
$y$	deflection induced by applied shear or moment
$\alpha$	angle of attack, deg
$\Delta$	maximum deflection of test vehicle, in.; m
$\Delta\varphi$	angle of bend for elemental beam length, rad
$\epsilon_1$	tensile strain, from bending and axial load only, in./in.; m/m
$\epsilon_2$	compression strain, from bending and axial load only, in./in.; m/m
$\theta$	half angle of unwrinkled portion of tank, deg
$\mu$	Poisson's ratio, in./in.; m/m

- $\sigma_{H,i}$  inside-surface hoop stress, psi;  $N/m^2$
- $\sigma_{H,o}$  outside-surface hoop stress, psi;  $N/m^2$
- $\sigma_{L,i}$  inside-surface longitudinal or bending stress, psi;  $N/m^2$
- $\sigma_{L,o}$  outside-surface longitudinal or bending stress, psi;  $N/m^2$

## TEST SETUP

The test vehicle for this program consisted of an Atlas LV-3C series (vehicle 116D) booster with the booster and sustainer engines removed. The Atlas LV-3C booster is a 120-inch- (3.05-m-) diameter, 563-inch- (14.3-m-) long, thin-walled cylinder with a dome-shaped bulkhead at the forward end and a conical-shaped aft end (fig. 2). An intermediate bulkhead divides the cylinder into a forward (oxidizer) tank and an aft (fuel) tank. The propellant tanks are constructed of 301 extra full-hard stainless-steel sheets varying in thickness from 0.014 inch (0.000356 m) at the forward end to 0.034 inch (0.000863 m) at the aft end. The steel sheets nominally 30 inches (0.761 m) in width are butt welded to form cylindrical bands. These bands are welded together circumferentially with lap joints to make up the total cylinder.

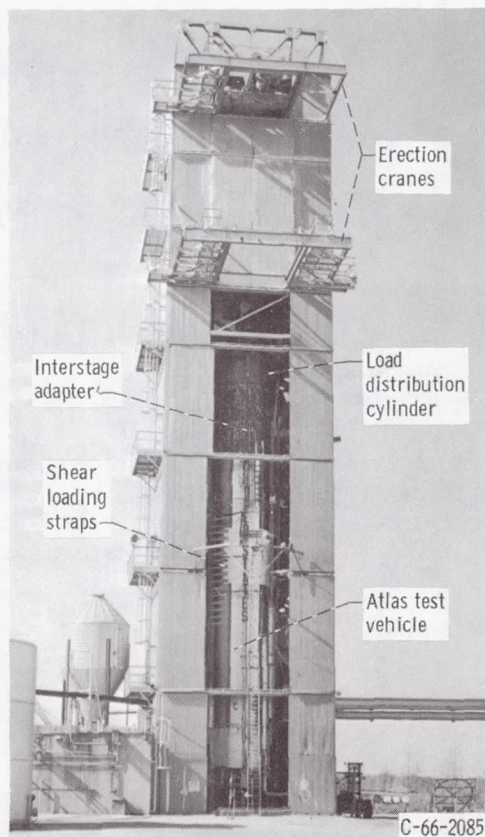
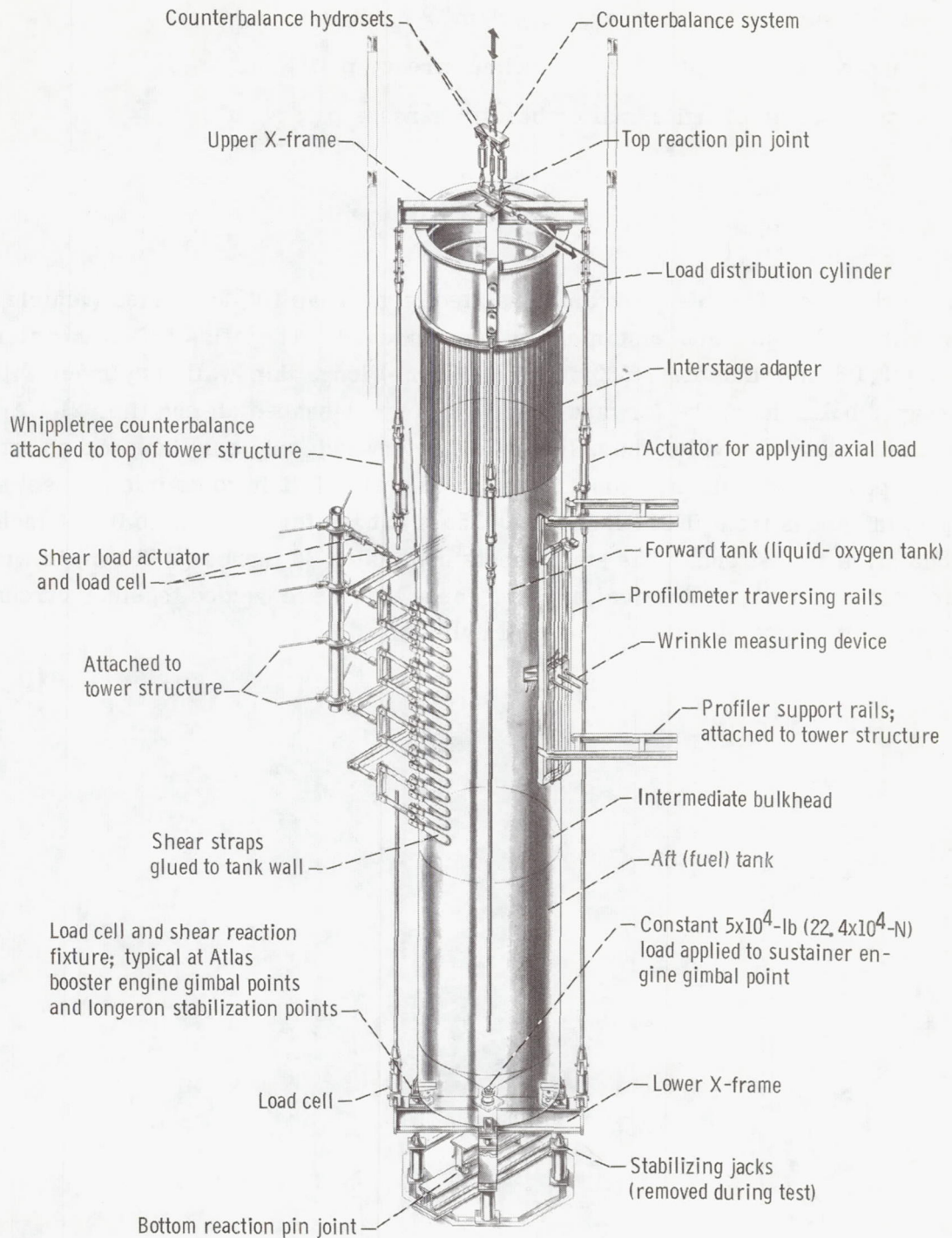
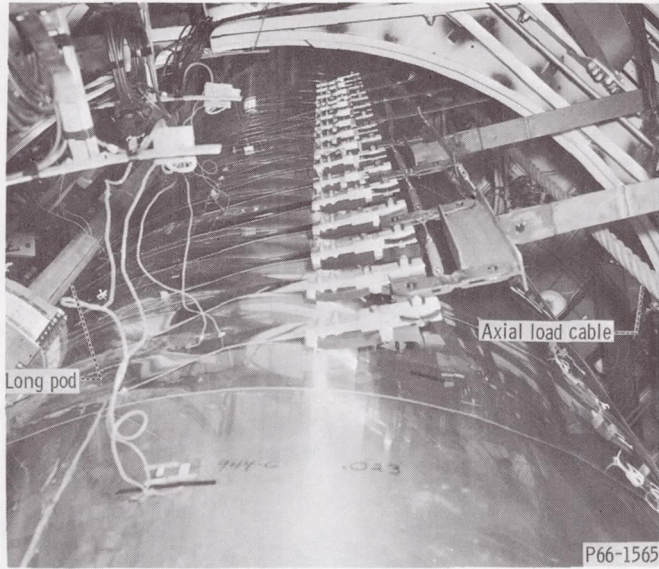


Figure 3. - Rocket Systems Dynamics Laboratory.

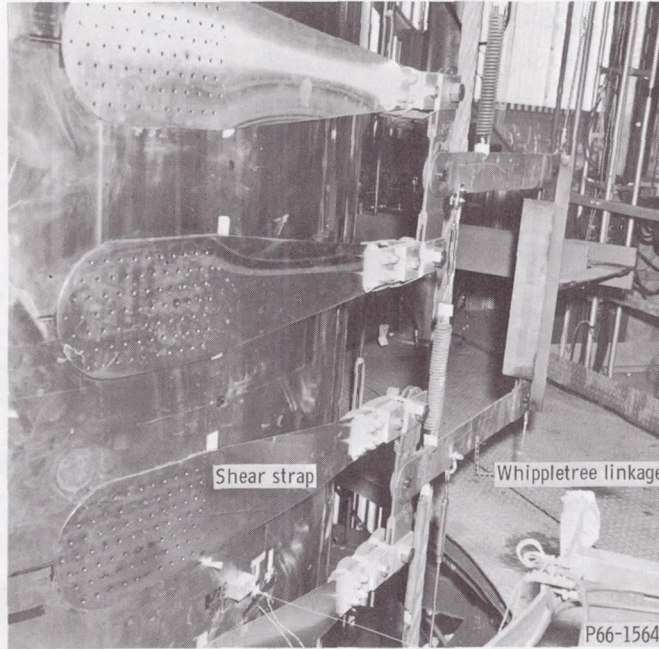


CD-8438-3I

Figure 4. - Postwrinkling-strength test setup for tests 1 and 2.



(a) View looking forward on Atlas liquid-oxygen tank.



(b) Shear-strap detail.

Figure 5. - Typical shear strap installation.

For testing, the Atlas booster was erected in the Rocket Systems Dynamics Laboratory (E tower), as shown in figure 3. The E tower is a 135-foot- (41.1-m-) high, 20-foot- (6.1-m-) square steel structure designed to accommodate an entire Atlas-Centaur vehicle.

A schematic of the test setup for the first two test conditions is shown in figure 4. The vehicle was mounted at the booster engine gimbal points and longeron support points

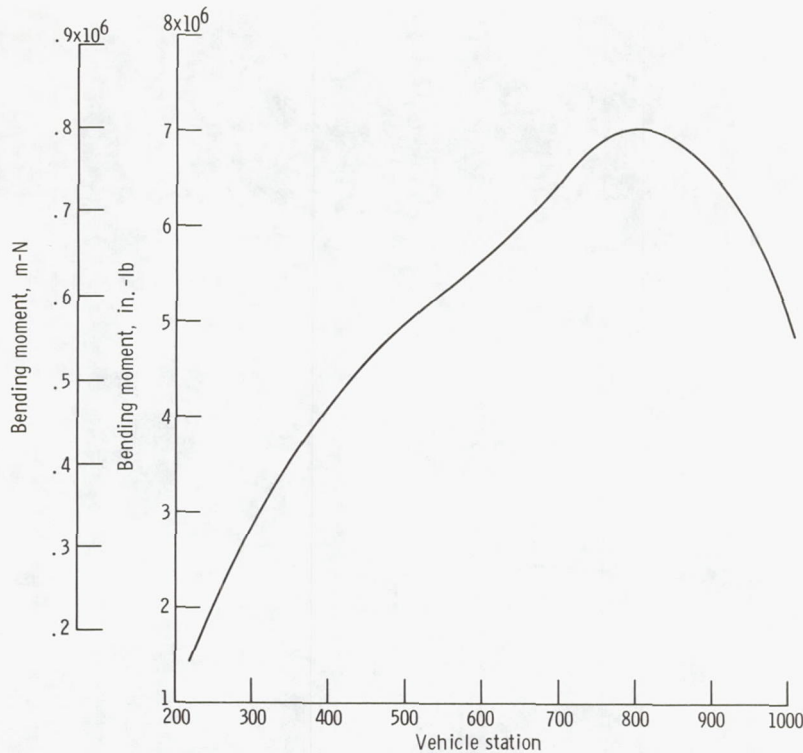
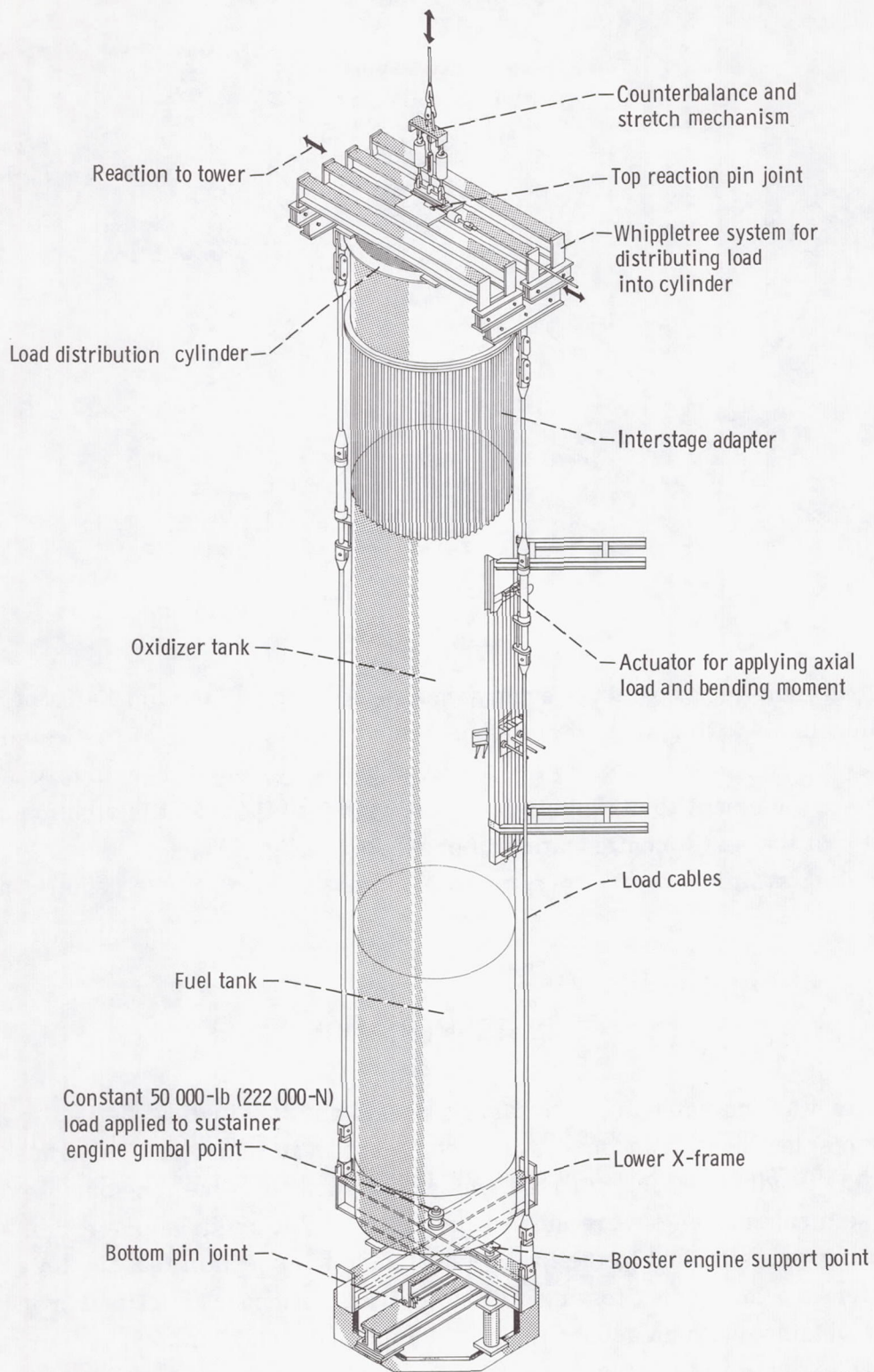


Figure 6. - Predicted bending moment as function of vehicle station at maximum value of product of angle of attack and aerodynamic pressure. Curve is based on typical March wind (see ref. 13).

to a heavy steel X-frame which in turn was attached to the floor of the tower through a pin joint. An X-frame was attached to the forward end of the vehicle through a heavy steel adapter cylinder and a flight configuration interstage adapter (used to mount the second-stage Centaur to the Atlas). The X-frame was joined to the tower structure through a pin joint that allowed free rotation and longitudinal motion. Axial compression load was applied through hydraulic actuators located in series with four cables strung the length of the vehicle and attached to the X-frames at each end of the test vehicle.

In the first two tests of the series, bending was achieved with shear loading applied to the Atlas. The shear load was induced through 16 pairs of steel straps glued along the neutral axis on each side of the oxidizer tank with an air-curing silicone rubber cement (see fig. 5). Loading of the straps was accomplished with four hydraulic actuators whiplight-connected to the glued-on straps. Hydraulic pressure to the four actuators was controlled through a proportioning device that allowed shaping the bending moment curve to approximate that predicted in flight (fig. 6).

To provide high bending moment over the entire length of the vehicle, as required for the third test, the shear straps were removed and bending was accomplished by differential loading of two cables strung the length of the vehicle. To distribute the con-



CD-10158-31

Figure 7. - Postwrinkling-strength test setup for test 3.

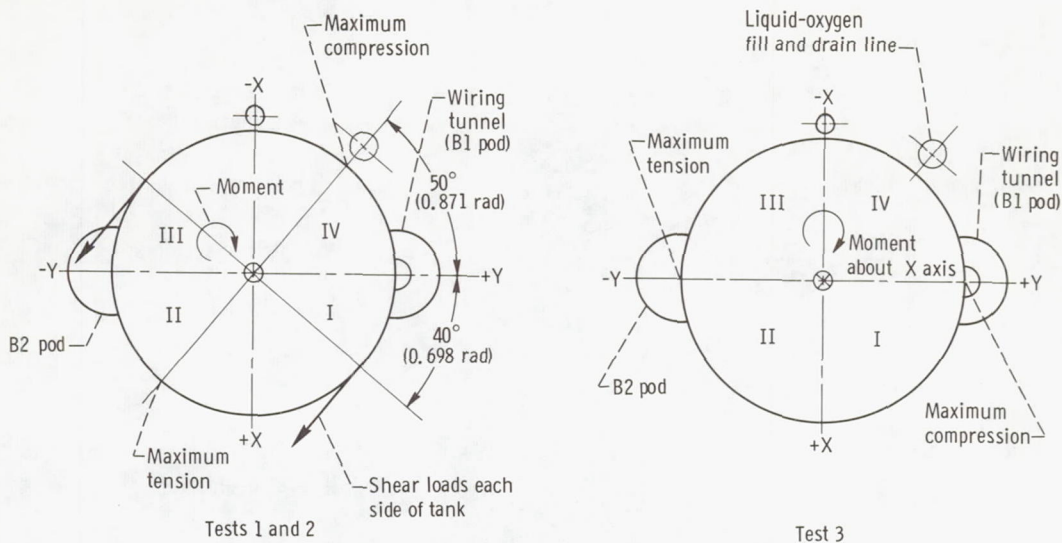


Figure 8. - Bending axis orientation.

centrated load from the two cables evenly into the Atlas tank, the top X-frame was removed and replaced with a system of beams placed across the top of the load distribution cylinder. The loading cables were attached to the system of beams through a whippetree arrangement to distribute the cable load into the load distribution cylinder. (A schematic of the test 3 configuration is presented in fig. 7).

The loading systems for the three tests oriented the loads to the vehicle, as shown in figure 8.

## INSTRUMENTATION

The Atlas was instrumented to measure lateral and longitudinal deflection with string-type displacement transducers located as shown in figure 9. The transducers for measuring the bending deflection of the tank were attached to the tension side of the tank wall. These measurements were made relative to the tower structure. Transit sightings of targets attached to the tower were made to ascertain that the tower provided a stable reference throughout testing. The electrical transducer deflection measurements were obtained with an accuracy of  $\pm 0.05$  inch ( $\pm 0.00127$  m).

In order to accurately define the mode of wrinkling in the tank wall, a remotely operated device (profilometer) was designed to measure the profile shape of the wrinkles (fig. 10). The wrinkle shapes were recorded on an X-Y plotter. The profilometer

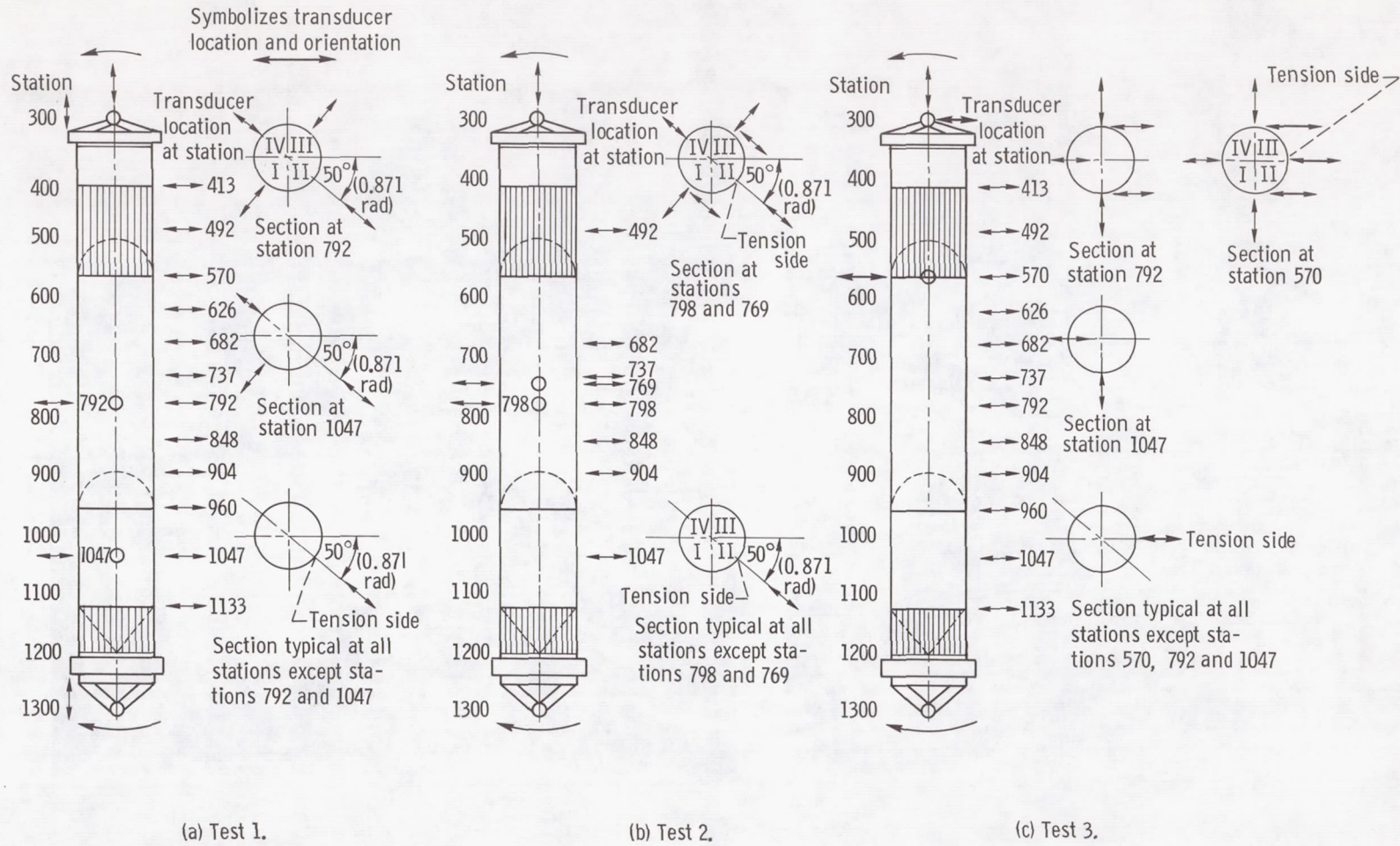
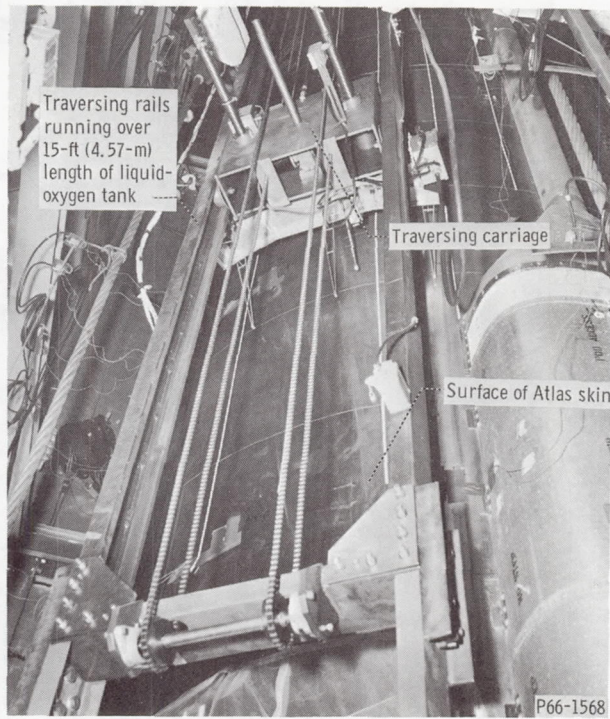
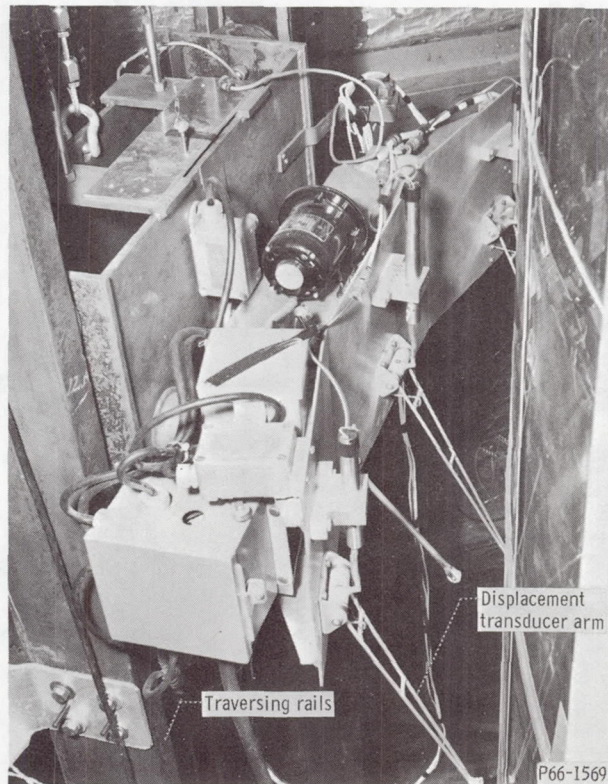


Figure 9. - Displacement transducer locations.



(a) Installation.



(b) Detail.

Figure 10. - Wrinkle-measuring-device (profilometer) installation.

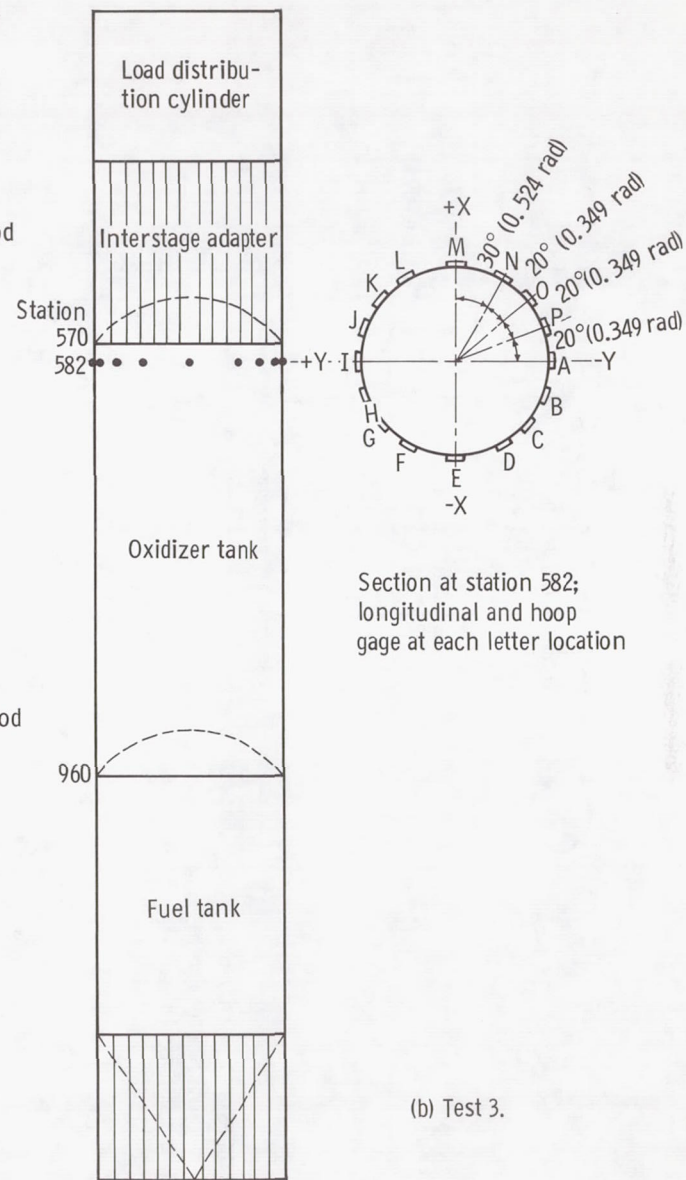
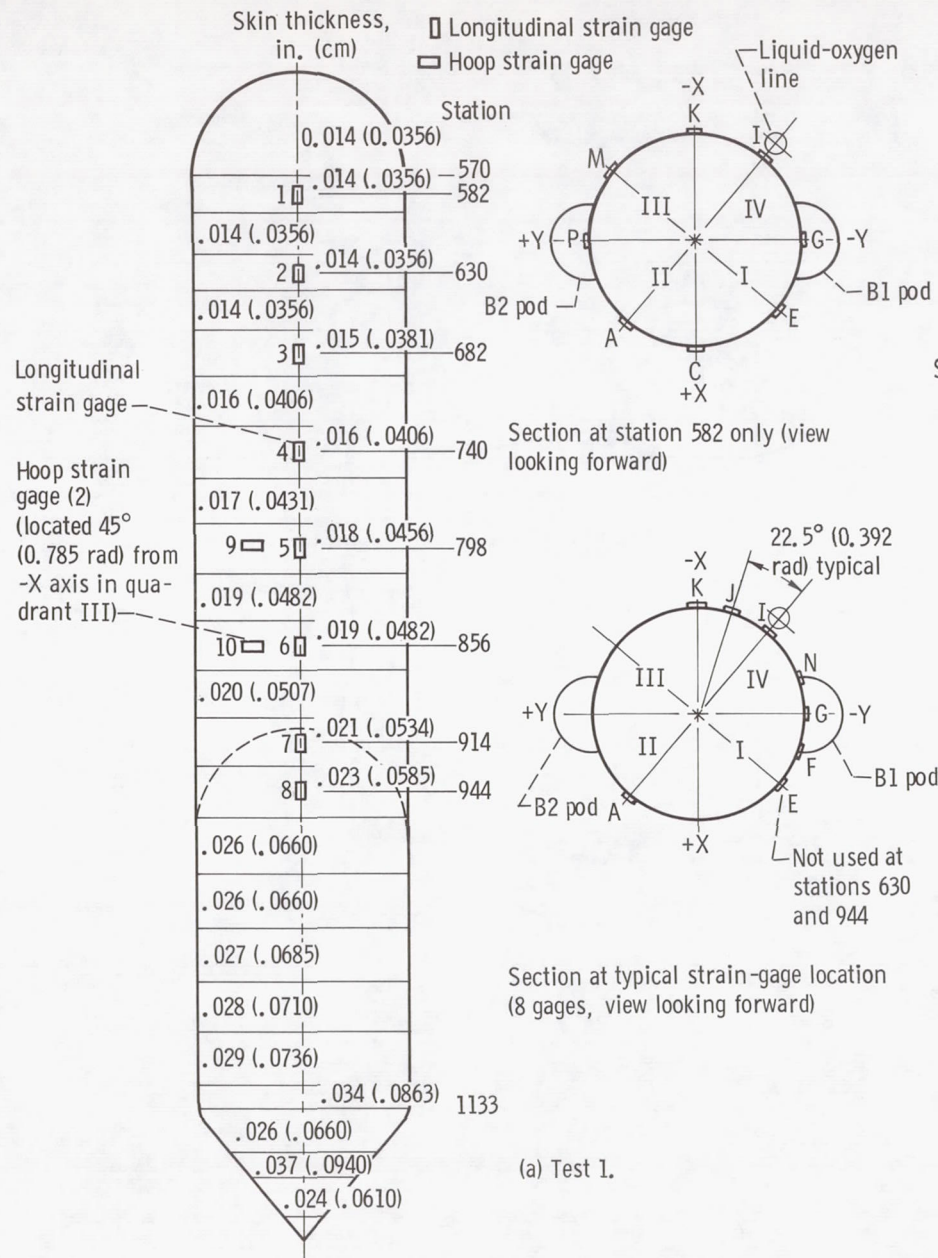


Figure 11. - Strain-gage locations.

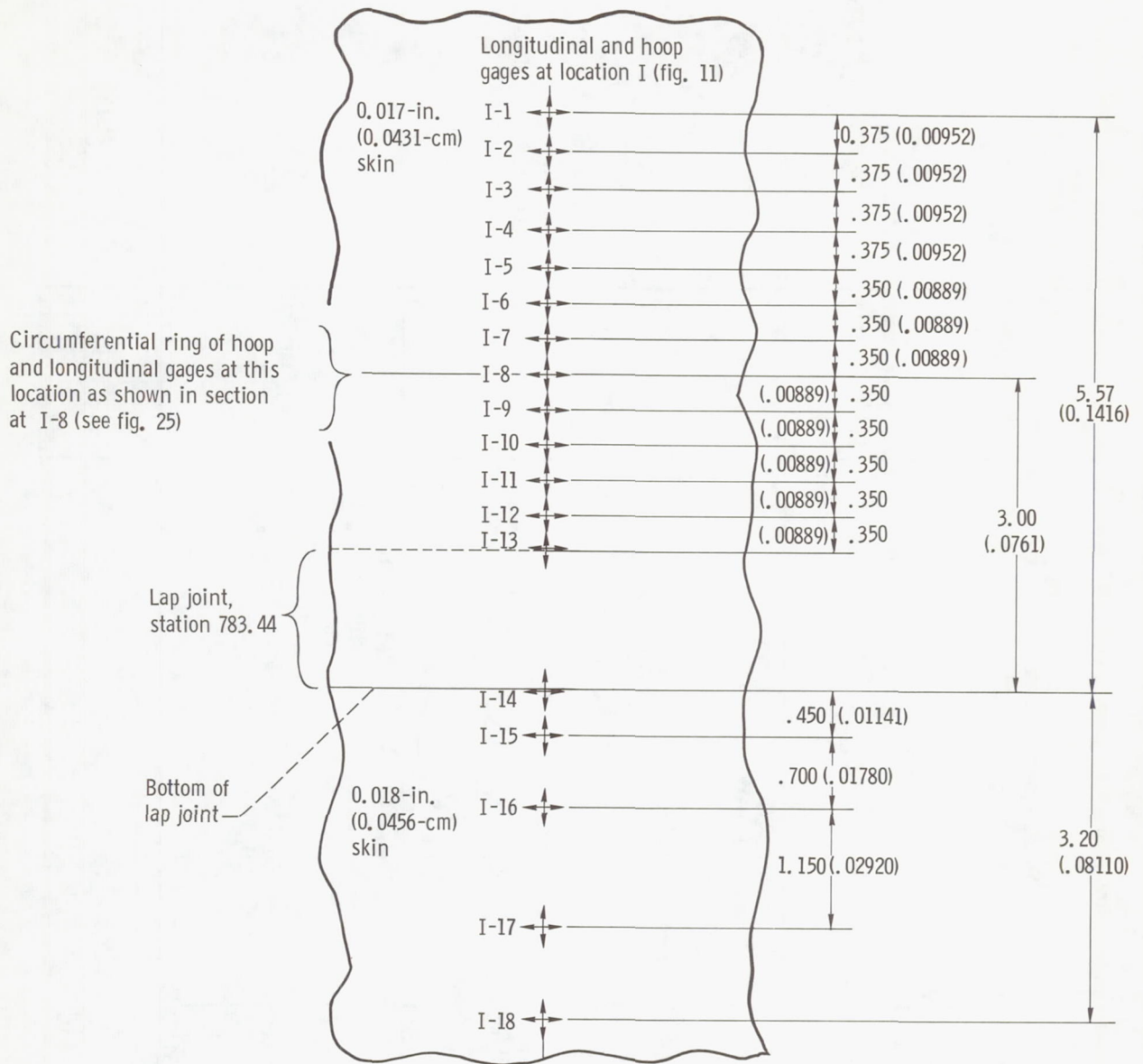


Figure 12. - Strain-gage locations for test 2. Dimensions are in inches (m).

mechanism was capable of traversing a 15-foot (4.56-m) length of the oxidizer tank in the area of maximum compression. The profilometer consisted of three displacement transducers mounted on a carriage that traversed the length of the oxidizer tank by means of guide rails and a chain-drive arrangement. The transducers sensed displacements through spring-loaded arms that maintained contact with the tank surface while the carriage traversed. The instrument was capable of being controlled to engage the tank wall while collecting data and to retract while loading was taking place. Profilometer traces of the tank wall were made after each loading condition was established.

For tests 1 and 2, strain gages were located on the outside surface of the tank wall around the circumference at various stations (see fig. 11). These gages were oriented to indicate both longitudinal and hoop strain.

For test 2, additional strain gages were placed over a point of high wrinkling as indicated by the profilometer in test 1. The gages were mounted on the outside surface of the tank in the area of the lap joint at station 783, as shown in figure 12. These gages gave an indication of the local hoop and bending strain in the wrinkles. All strain measurements were made with an accuracy of  $\pm 70$  microinches per inch ( $\pm 1.78 \mu\text{m}/\text{m}$ ).

All testing was controlled remotely from a central control building approximately 1/4 mile (402 m) from the test tower to eliminate the hazard from a potential tank rupture. Remotely operated cameras recorded pictures of the test vehicle at selected increments of loading. Continuous surveillance of the Atlas was maintained from the control building by means of television cameras and through high-power telescopes located 250 feet (76 m) from the test tower.

The strain-gage, displacement-transducer, and load-cell outputs were recorded on magnetic tape through an analog-to-digital converter at the control building.

## TEST PROCEDURE

The test procedures for tests 1 and 2 were essentially the same, except that the bending in test 2 was taken to the full moment capability of the oxidizer tank. The Atlas was first filled with water and pressurized, the fuel tank to 58.5 psig ( $403\,000 \text{ N}/\text{m}^2$  gage) and the oxidizer tank to 24 psig ( $165\,000 \text{ N}/\text{m}^2$  gage). An axial compressive load of 75 800 pounds (336 000 N) was applied and held constant throughout each of the first two tests. The bending was accomplished through loading of the shear straps. Bending moment was applied in one-million-inch-pound ( $0.113 \times 10^6$  -m-N) increments with data being recorded at each stabilized load increment. The applied bending moment was defined by the shear strap loads acting through the geometry of the test setup. A load cell, mounted in conjunction with the top pin connection, gave verification of the applied

shear through its reaction. The shear loads were measured with an accuracy of 150 pounds (665 N) by load cells located in series between each hydraulic actuator and its corresponding set of straps.

During test 1 the moment load was increased and then dropped back to a base level ( $4 \times 10^6$  in.-lb, or  $0.451 \times 10^6$  m-N) that was well below the wrinkling onset point, in order to investigate the repeatability of the loadings and deflection. For test 2 the load was increased in increments to the maximum level ( $10.2 \times 10^6$  in.-lb, or  $1.15 \times 10^6$  m-N) without returning to the base value.

A continuous plot of deflection against bending moment at station 798 in the oxidizer tank was maintained during the test. These values were compared with predicted values as a primary indication of bending capability remaining before the next increment of load was applied. At each load, data from the profilometer were studied as a check of the severity of the skin wrinkles. Key strain gages were also monitored during the test to measure distribution of load into the vehicle.

The procedure for test 3 followed that for the first two tests, with the following exceptions. The oxidizer tank pressure was set at the flight pressure of 28.5 psig ( $196\,000$  N/m<sup>2</sup> gage), and the axial load was maintained at the simulated flight axial load of 126 000 pounds (559 000 N). The shear straps were removed, and a constant bending moment was induced over the entire length of the tank by differential loading of two longitudinal cables in the Y, Z plane. In this manner a couple was induced that essentially applied a constant moment over the length of the Atlas and adapters. The same procedure for monitoring the test progress was followed as for tests 1 and 2.

## RESULTS AND DISCUSSION

The test program consisted of three tests. Each test essentially fulfilled one of the three basic objectives of the program.

The first test (test 1) of the series was designed to verify the postwrinkling behavior of the full-scale Atlas vehicle as indicated by analysis and previous model testing (refs. 2 and 3).

The maximum bending load applied in test 1 is shown in figure 13, along with the measured and predicted deflection of the vehicle for the peak load condition. (The method of obtaining the analytical deflections is presented in appendix A of this report.) The maximum moment applied was  $10.2 \times 10^6$  inch-pounds ( $1.15 \times 10^6$  m-N) at station 810. This moment is approximately 50 percent higher than the predicted wrinkling onset load designated by the dashed line in figure 13. The comparison of predicted and measured deflection indicates that the beam deflection of the wrinkled Atlas vehicle can be predicted with reasonable accuracy.

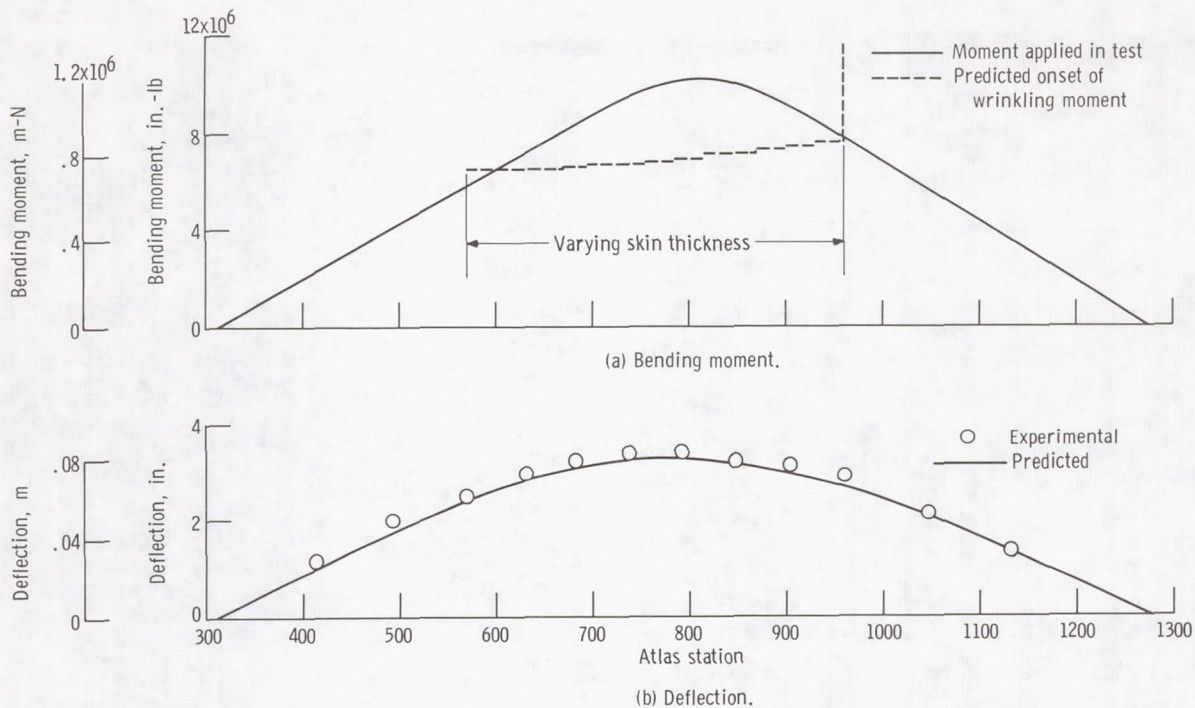


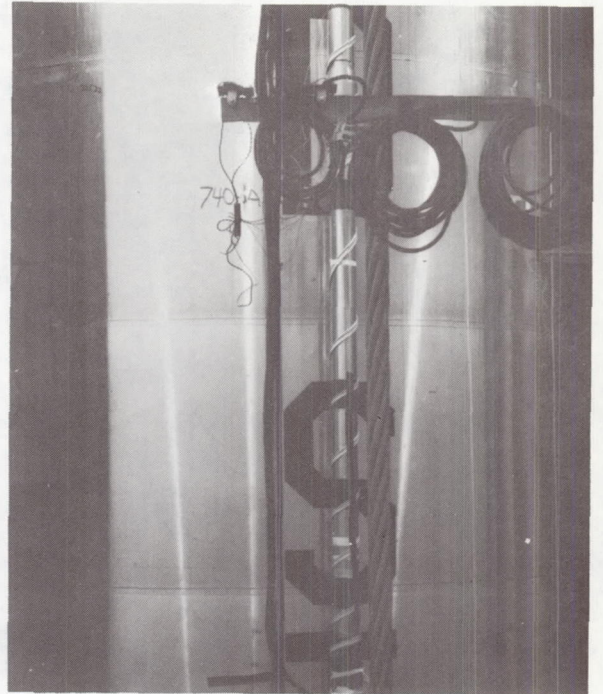
Figure 13. - Bending moment and deflection as function of Atlas station - test 1. Test conditions: axial load, 75 800 pounds (336 000 N); oxidizer tank pressure, 24.0 psig (165 000 N/m<sup>2</sup>); fuel tank pressure, 58.5 psig (402 500 N/m<sup>2</sup>); oxidizer tank filled with water to station 540; fuel tank filled with water to station 925.

As the moment was increased beyond the onset of skin wrinkling the buckles appeared as damped sinusoidal waves propagating from the lap joint areas and progressing toward the middle portion of the tank skins (see fig. 14). The profile of the tank surface at the extreme compression fiber is shown in figure 15 under the influence of several test 1 loading conditions.

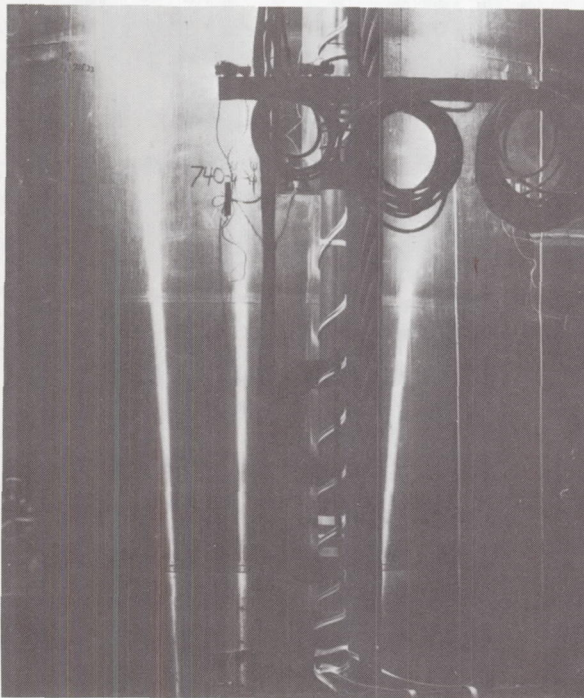
The stress distribution around the tank circumference as measured with strain gages is compared with predicted distribution in figure 16. The analytical load or stress distribution around the tank was obtained by using the equations presented in appendix B of this report. The stress or load distribution around the circumference of the tank is in reasonable agreement with theory. A plot of deflection against bending moment, both predicted and experimental, at the station of maximum moment is shown in figure 17. The deflection data points are numbered to indicate the sequence in which they were acquired and to illustrate the effect of reducing the moment to the base value before proceeding to the next higher load increment. The linearity in repeating the wrinkling loads was reasonably good with the deflection repeating at the base load within 0.2 inch (0.00507 m). It is believed that at least half of this value was the result of taking up test fixture slack and of self-alignment.



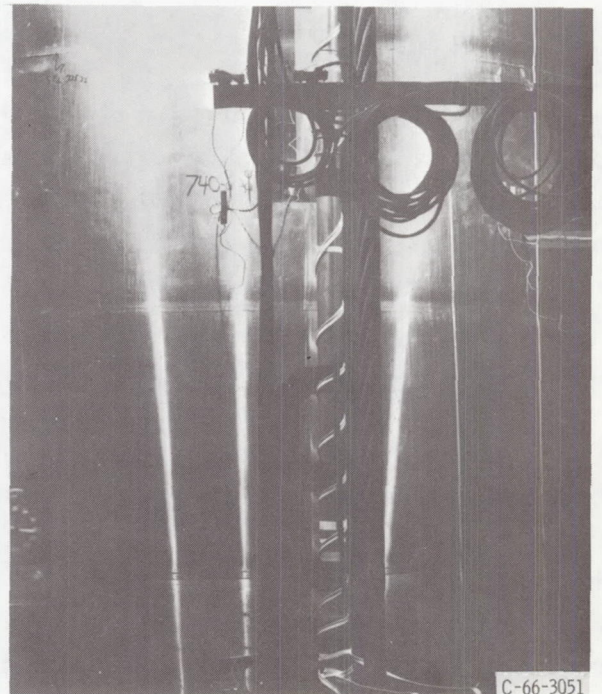
(a) Axial load only.



(b) Bending moment,  $4.23 \times 10^6$  inch-pounds ( $0.476 \times 10^6$  m-N).

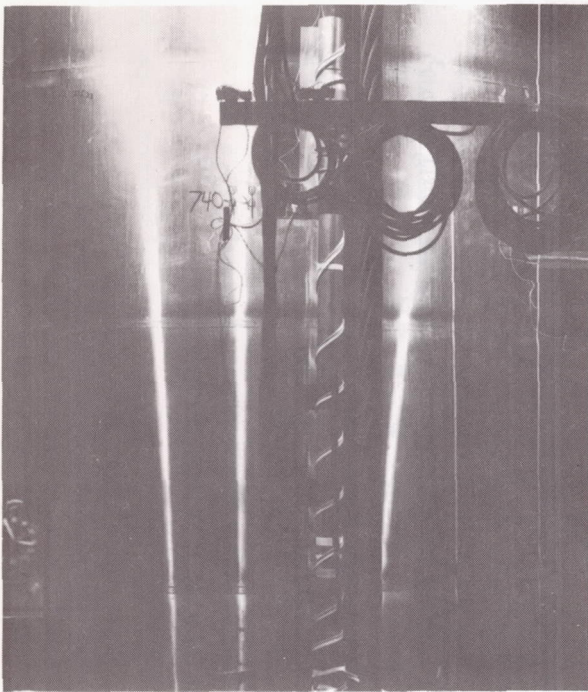


(c) Bending moment,  $7.42 \times 10^6$  inch-pounds ( $0.837 \times 10^6$  m-N).

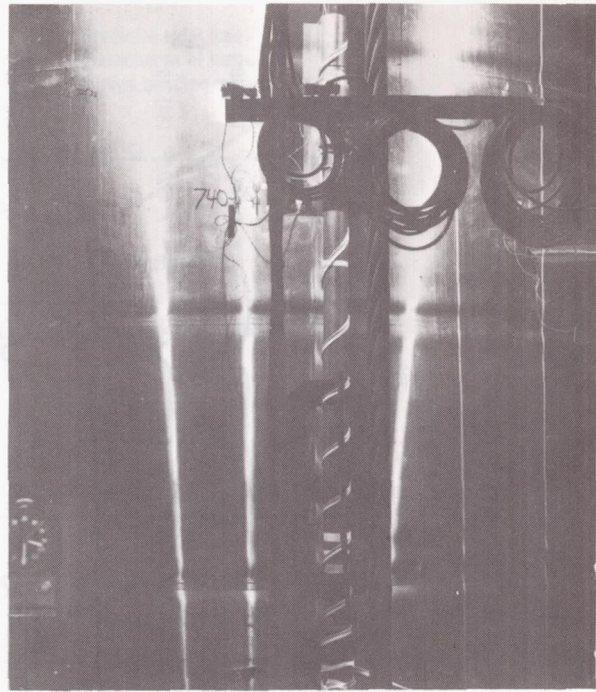


(d) Bending moment,  $7.96 \times 10^6$  inch-pounds ( $0.900 \times 10^6$  m-N).

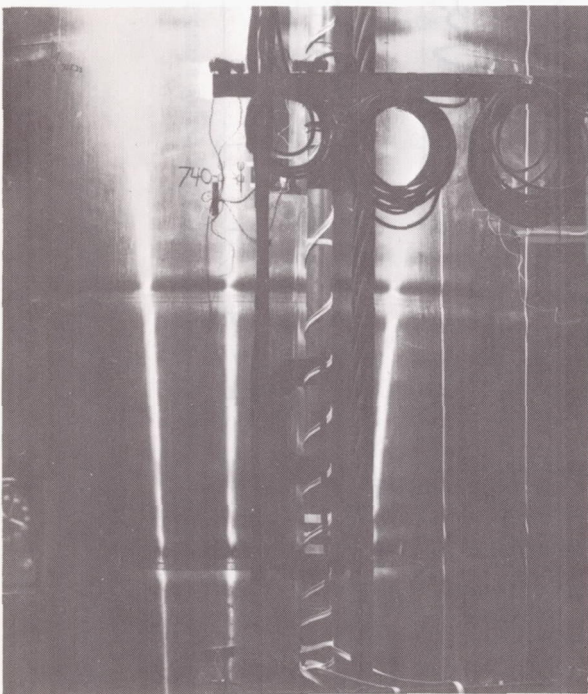
Figure 14. - Wrinkle patterns for test 1. Axial load, 75 800 pounds (336 000 N).



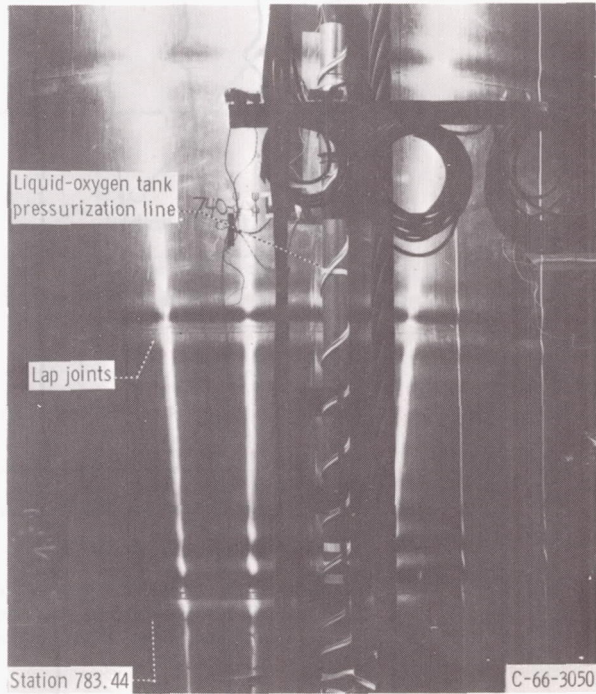
(e) Bending moment,  $8.51 \times 10^6$  inch-pounds ( $0.961 \times 10^6$  m-N).



(f) Bending moment,  $9.06 \times 10^6$  inch-pounds ( $1.023 \times 10^6$  m-N).

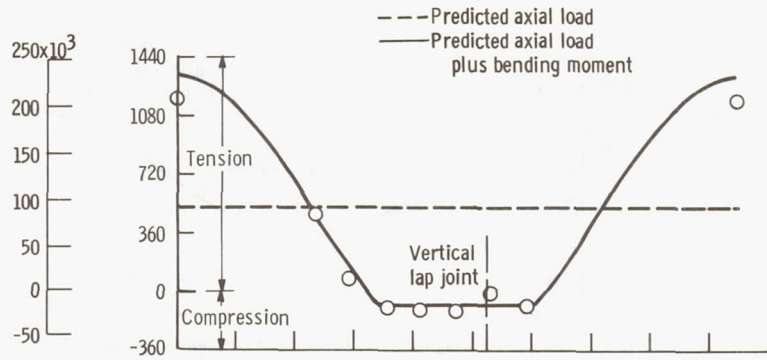


(g) Bending moment,  $9.62 \times 10^6$  inch-pounds ( $1.089 \times 10^6$  m-N).

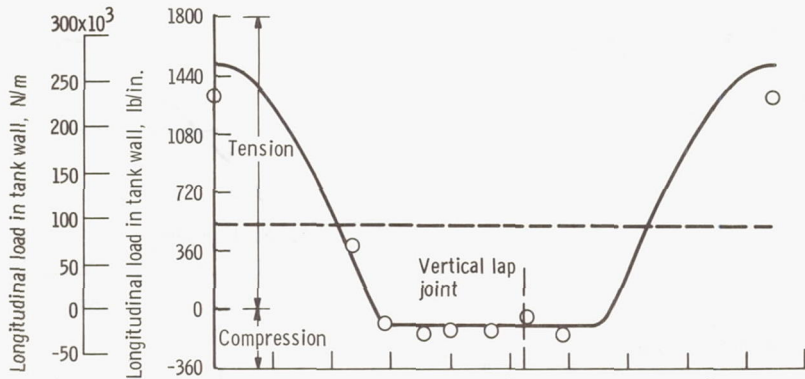


(h) Bending moment,  $10.22 \times 10^6$  inch-pounds ( $1.158 \times 10^6$  m-N).

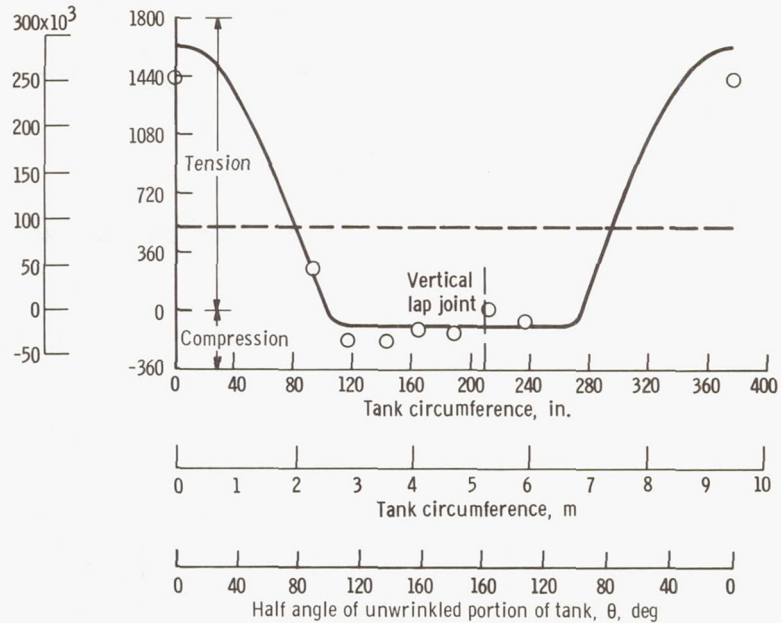
Figure 14. - Concluded.



(d) Bending moment,  $8.51 \times 10^6$  inch-pounds ( $956 \times 10^3$  m-N).



(e) Bending moment,  $9.62 \times 10^6$  inch-pounds ( $1089 \times 10^3$  m-N).



(f) Bending moment,  $10.22 \times 10^6$  inch-pounds ( $1157 \times 10^3$  m-N).

Figure 16. - Concluded.

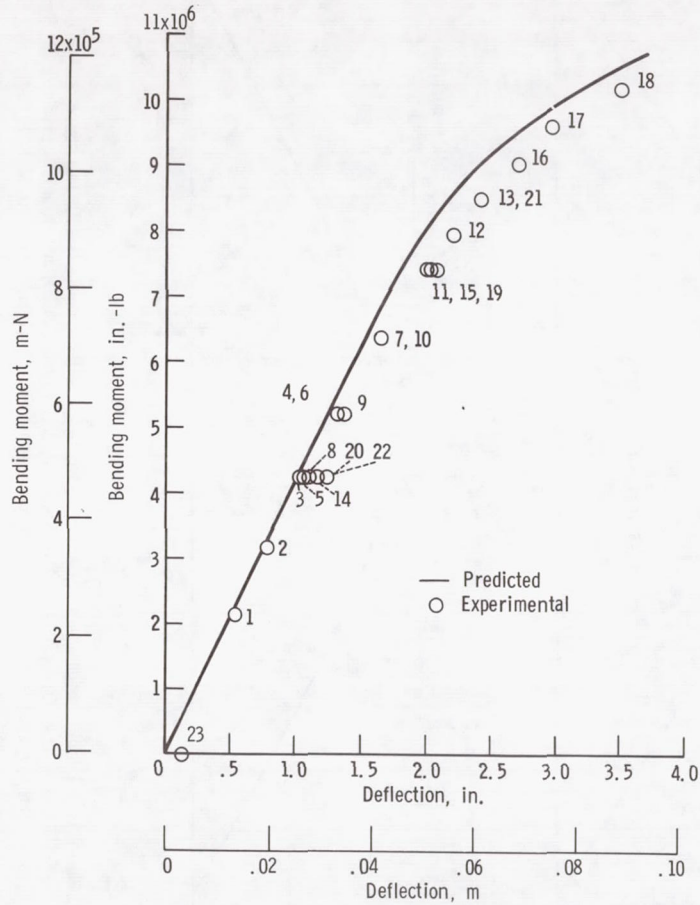


Figure 17. - Comparison of theoretical deflection with data at station 792. Test 1; repeated loading; axial load, 75 800 pounds (336 000 N). (Numbers accompanying data points indicate sequence of load application.)

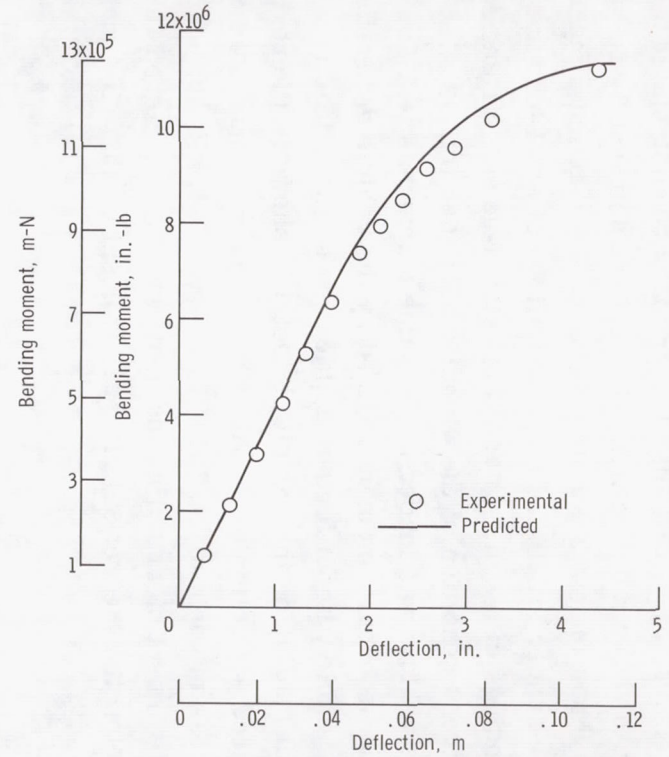


Figure 18. - Comparison of theoretical deflection with data at station 798 (approx. middle of oxidizer tank). Test 1; repeated loading; axial load, 75 800 pounds (336 000 N).

The results of test 1 indicate that the behavior of the Atlas structure under the influence of postwrinkling bending loads follows the analysis of reference 1 and the findings of model tests (refs. 2, 3, 5, and 10) as to primary bending stability, mode and extent of skin wrinkling, and beam deflection. (More details of test 1 are presented in ref. 10.)

The specific intent of test 2 was to determine the maximum moment capability of the Atlas oxidizer tank under simulated flight conditions of axial load and tank pressure and to confirm the findings of test 1. In addition, strain-gage instrumentation was applied to study the local stress condition of the wrinkled skin (see fig. 12).

In test 2, the vehicle was loaded in the same manner as test 1. The loading was continued until the secondary moment induced by the vehicle deflection was sufficient to make the beam unstable without further application of shear load (see fig. 18). The maximum moment loading on the vehicle in test 2 is shown in figure 19(a), and the predicted and measured deflection of the Atlas under the maximum load condition in figure 19(b). The peak moment of  $11.2 \times 10^6$  inch-pounds ( $1.265 \times 10^6$  m-N) is 63 percent above the predicted onset of wrinkling moment, shown as a dashed line in figure 19(a), and 17 percent below the theoretical ultimate moment of  $13.5 \times 10^6$  inch-pounds

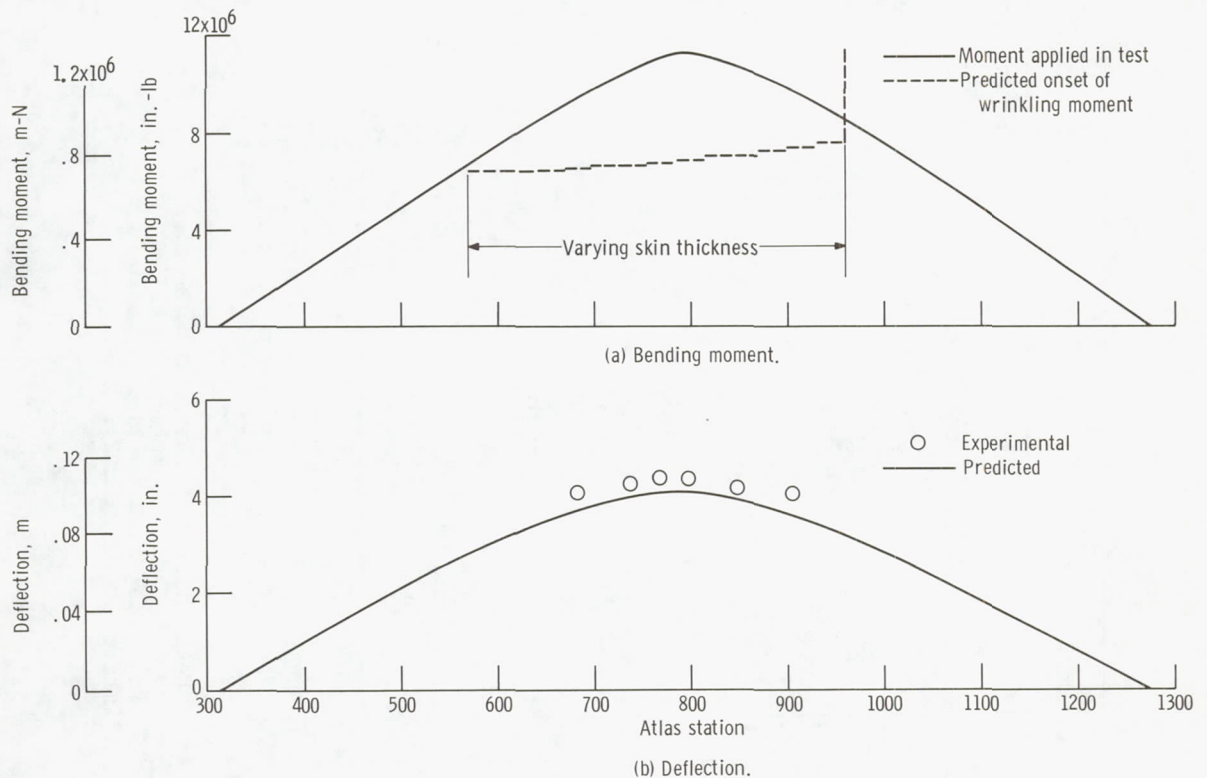


Figure 19. - Bending moment and deflection as function of Atlas station - test 2. Test conditions: axial load, 75 800 pounds (336 000 N); oxidizer tank pressure, 24.0 psig (165 000 N/m<sup>2</sup>); fuel tank pressure, 58.5 psig (402 500 N/m<sup>2</sup>); oxidizer tank filled with water to station 540; fuel tank filled with water to station 925.

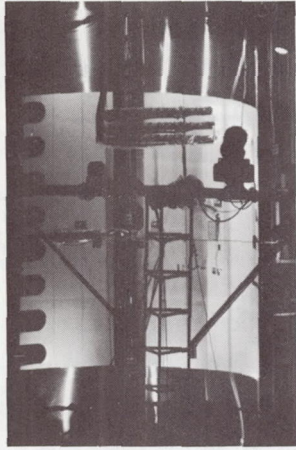
( $1.525 \times 10^6$  m-N) (ref. 1), which would have produced wrinkles around the entire circumference of the tank. The  $11.2 \times 10^6$ -inch-pound ( $1.265 \times 10^6$ -m-N) moment produces wrinkling around approximately 20% of the tank circumference. The peak bending moment was reached, however, before the wrinkles enveloped the entire tank circumference. This occurred when the shallow damped sinusoidal wrinkle pattern abruptly shifted to a few deep wrinkles concentrated at one lap joint (see fig. 20). This abrupt shift of wrinkle pattern was also observed in the testing of reference 5.

Test 2 was terminated when static equilibrium could no longer be maintained, and all loads were immediately removed to prevent destruction of the test vehicle. Typical wrinkle patterns observed during test 2 are shown in both figures 20 and 21. In figure 21, skin wrinkling can be observed under the wiring tunnel. The presence of the tunnel had no apparent effect on the wrinkling pattern nor was any damage to the tunnel and its attachments observed.

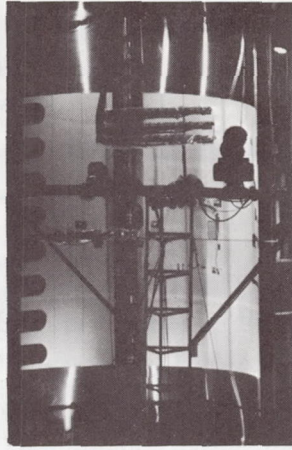
The stress levels measured at station 783 are presented in figure 22. In this figure the hoop and longitudinal stresses at the extreme compression fiber are compared with the buckle profile as established with the profilometer in the instrumented area. The figure presents a progression of stress level as the test loads were applied. The stress values were derived from the biaxial strain readings using modulus of elasticity values of  $25.5 \times 10^6$  and  $29.3 \times 10^6$  psi ( $175 \times 10^9$  and  $202 \times 10^9$  N/m<sup>2</sup>), respectively, for the hoop and longitudinal directions.

The bending moment capability of the test vehicle is illustrated in figure 18. Figure 23(a) compares the principal stresses on the outside surface of the tank with applied moment. The stress values were those obtained at the most highly stressed point in the wrinkled area at station 783. The peak stresses occurred in the first outward wrinkle above the lap joint at station 783. All stresses were obtained from strain-gage instrumentation on the outside surface of the tank skin. As bending moment was applied to the vehicle, the hoop stress remained relatively constant until the onset of skin wrinkling. After wrinkling the hoop stress increased linearly with moment. As the vehicle was bent, the longitudinal skin tension induced by the tank pressure was relieved on the compression side until the skin began to wrinkle. As wrinkling began, the longitudinally oriented gages indicated increasing tension, primarily from local bending of the skin in the area instrumented. The longitudinal stress assumed a linear relation with moment after the onset of wrinkling.

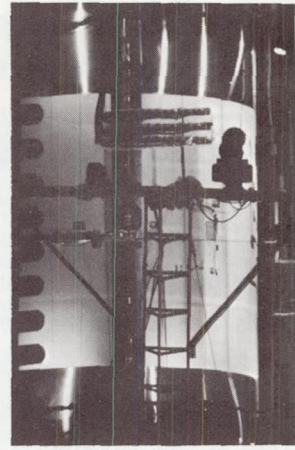
Figure 23(b) presents the corresponding stress conditions on the inside surface of the tank wall. These values were calculated by using the experimental strain data collected on the outside surface. The calculations were made as follows:



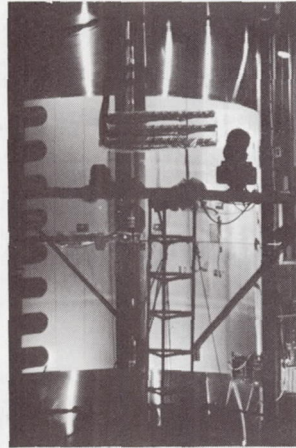
(a) Bending moment,  $6.35 \times 10^6$  inch-pounds ( $716 \times 10^3$  m-N).



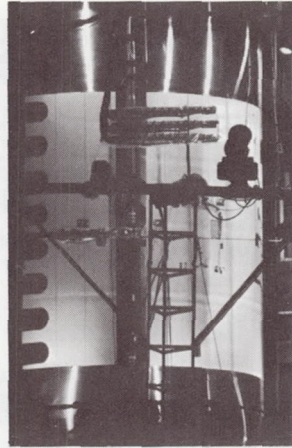
(b) Bending moment,  $7.4 \times 10^6$  inch-pounds ( $835 \times 10^3$  m-N).



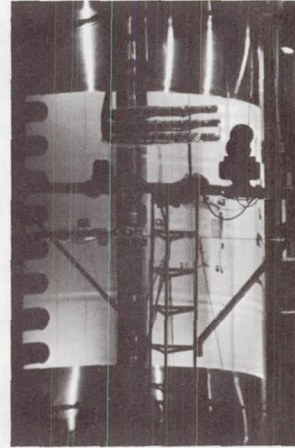
(c) Bending moment,  $7.95 \times 10^6$  inch-pounds ( $898 \times 10^3$  m-N).



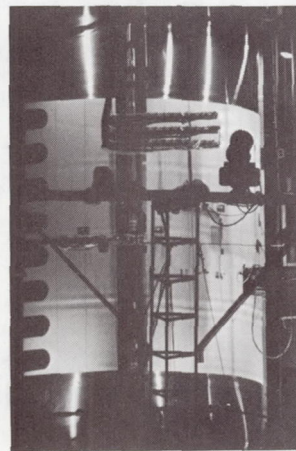
(d) Bending moment,  $8.5 \times 10^6$  inch-pounds ( $960 \times 10^3$  m-N).



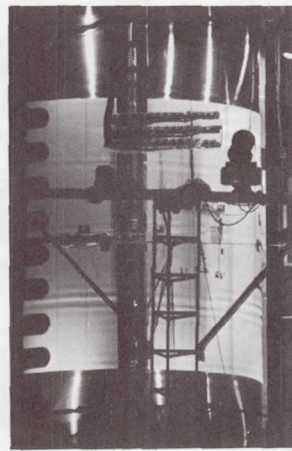
(e) Bending moment,  $9.05 \times 10^6$  inch-pounds ( $1021 \times 10^3$  m-N).



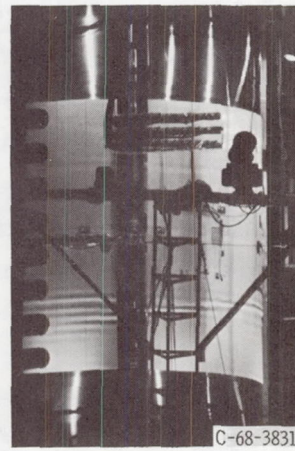
(f) Bending moment,  $9.6 \times 10^6$  inch-pounds ( $1085 \times 10^3$  m-N).



(g) Bending moment,  $10.15 \times 10^6$  inch-pounds ( $1146 \times 10^3$  m-N).

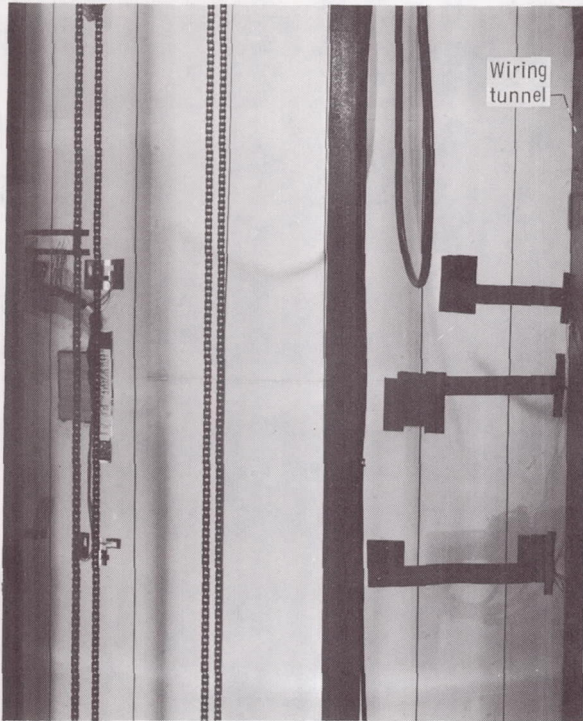


(h) Bending moment,  $10.9 \times 10^6$  inch-pounds ( $1230 \times 10^3$  m-N).

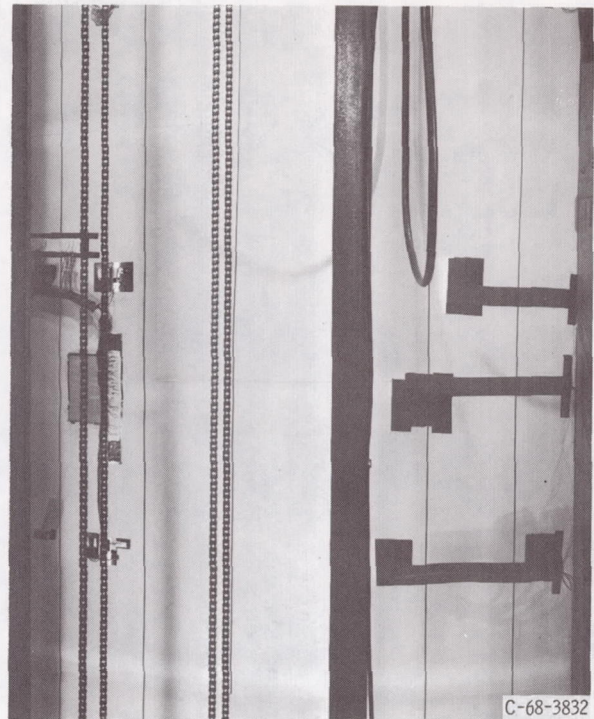


(i) Bending moment,  $11.04 \times 10^6$  inch-pounds ( $1250 \times 10^3$  m-N).

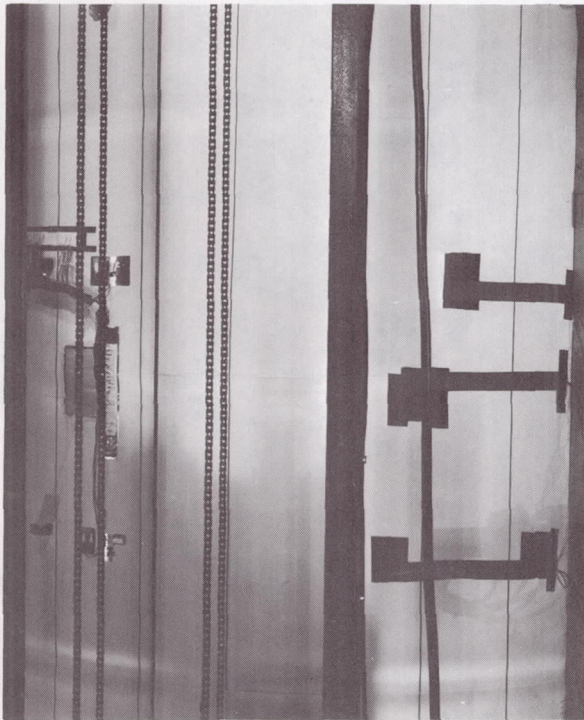
Figure 20. - Wrinkle patterns - test 2.



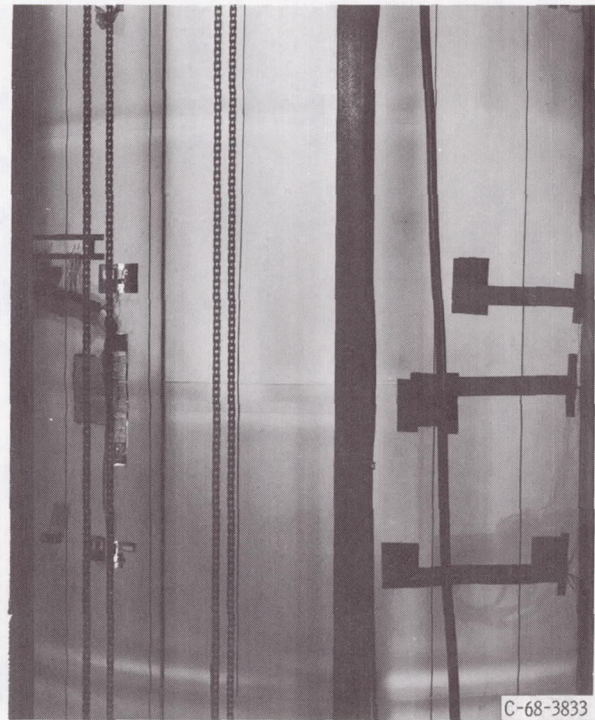
(a) Bending moment,  $6.35 \times 10^6$  inch-pounds ( $716 \times 10^3$  m-N).



(b) Bending moment,  $7.4 \times 10^6$  inch-pounds ( $835 \times 10^3$  m-N).

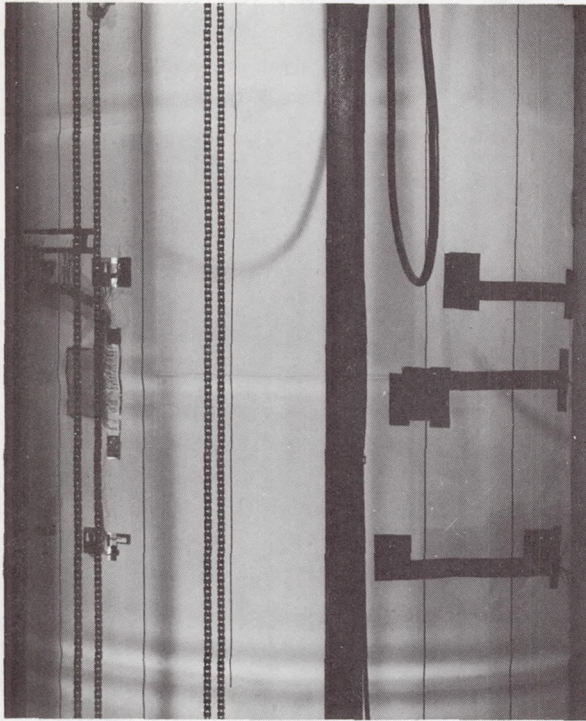


(c) Bending moment,  $7.95 \times 10^6$  inch-pounds ( $898 \times 10^3$  m-N).

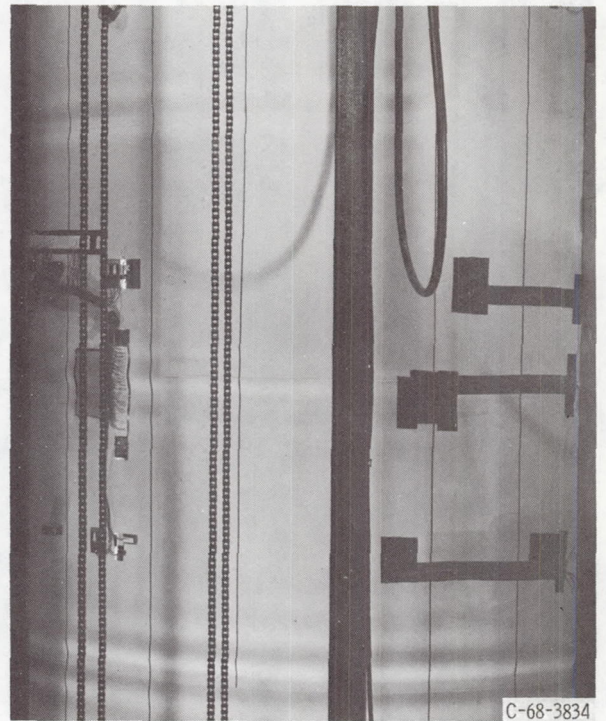


(d) Bending moment,  $8.5 \times 10^6$  inch-pounds ( $960 \times 10^3$  m-N).

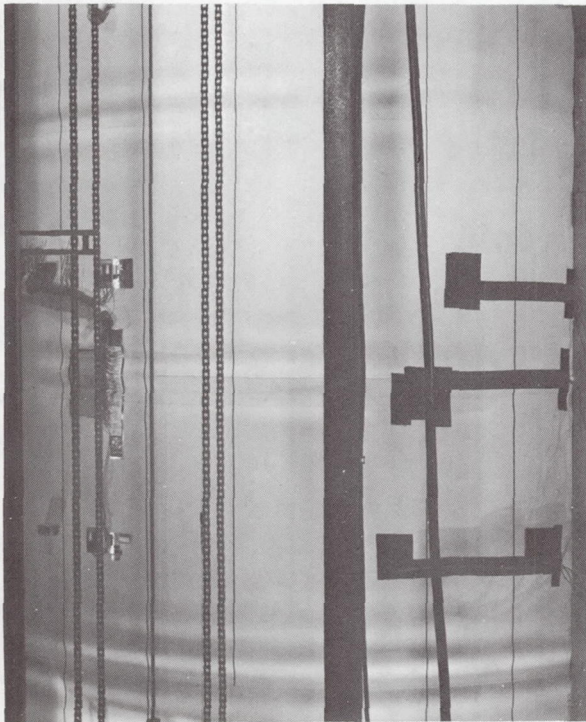
Figure 21. - Closeup of wrinkle patterns - test 2.



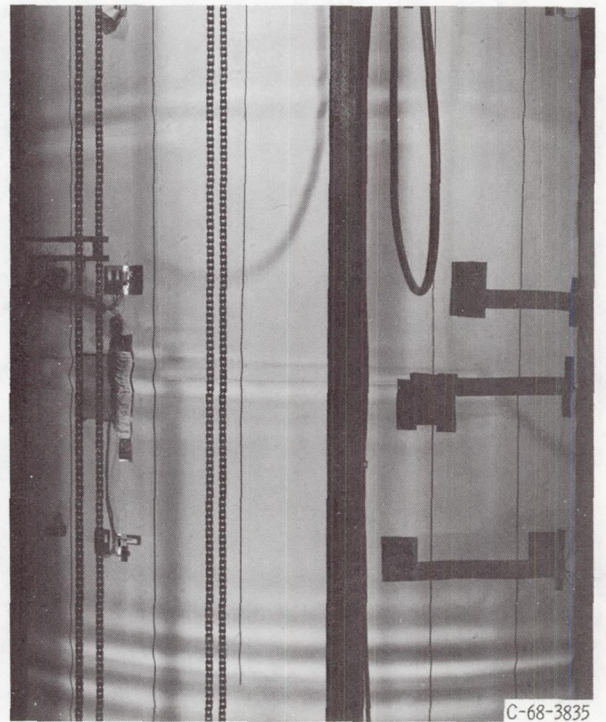
(e) Bending moment,  $9.05 \times 10^6$  inch-pounds ( $1021 \times 10^3$  m-N).



(f) Bending moment,  $9.6 \times 10^6$  inch-pounds ( $1085 \times 10^3$  m-N).



(g) Bending moment,  $10.15 \times 10^6$  inch-pounds ( $1146 \times 10^3$  m-N).



(h) Bending moment,  $10.9 \times 10^6$  inch-pounds ( $1230 \times 10^3$  m-N).

Figure 21. - Concluded.

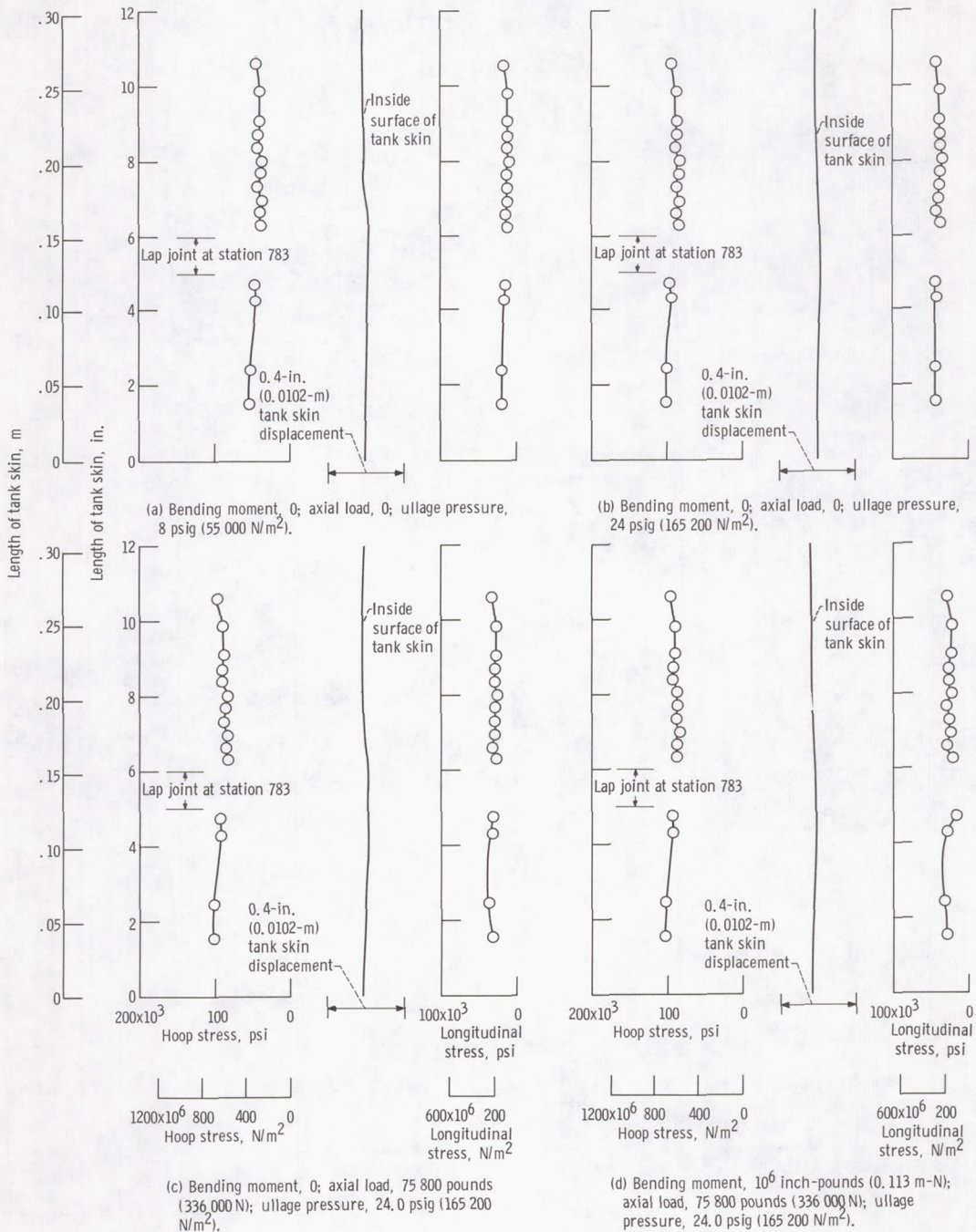


Figure 22. - Atlas postwrinkling-strength test. Comparison of wrinkle shape, longitudinal stress, and hoop stress at maximum compression fiber. Hydrostatic head, 213 inches (5.4 m) of water.

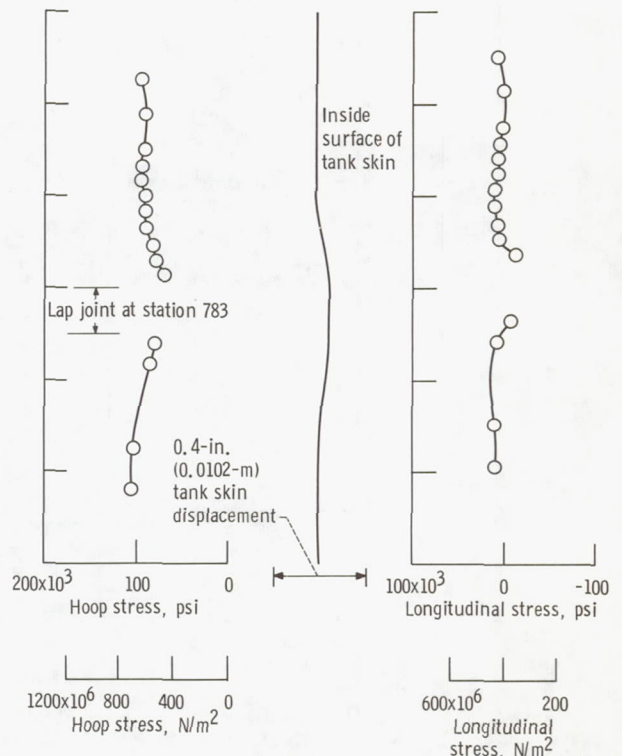
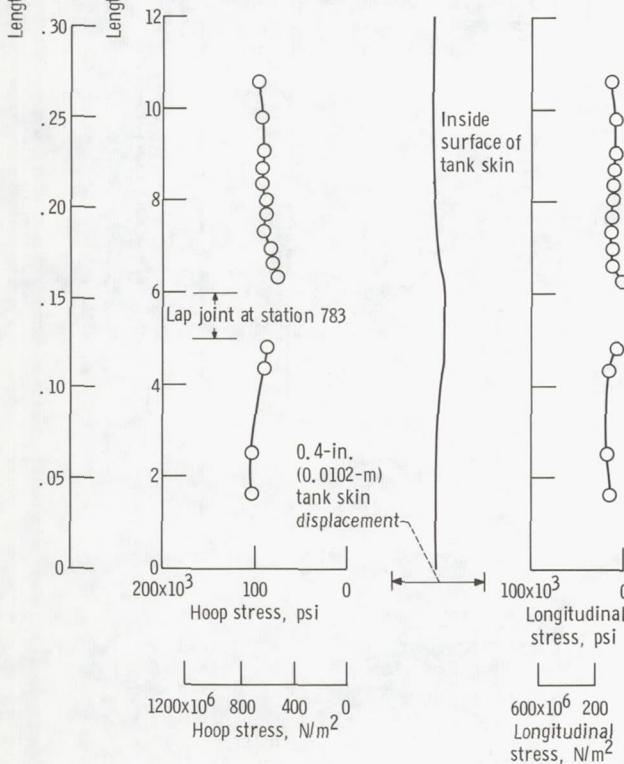
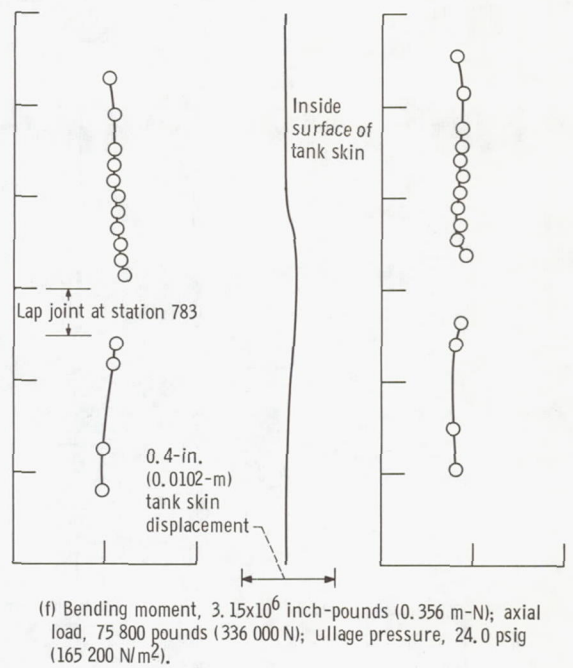
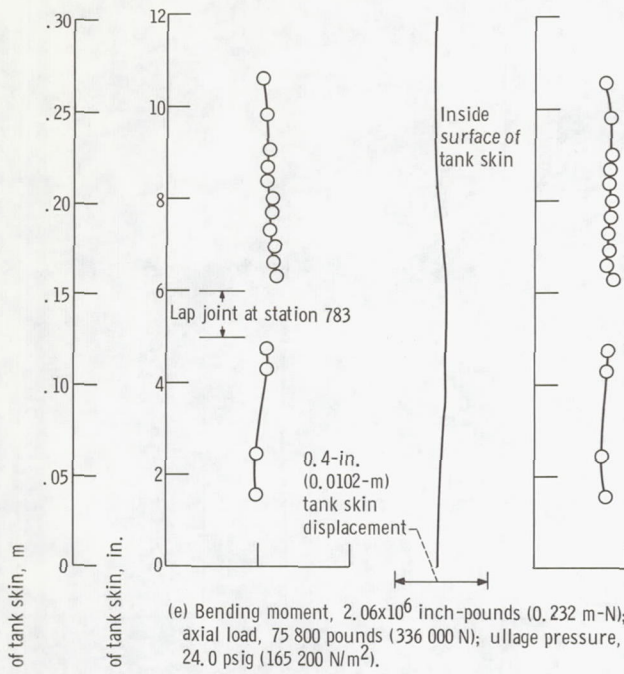
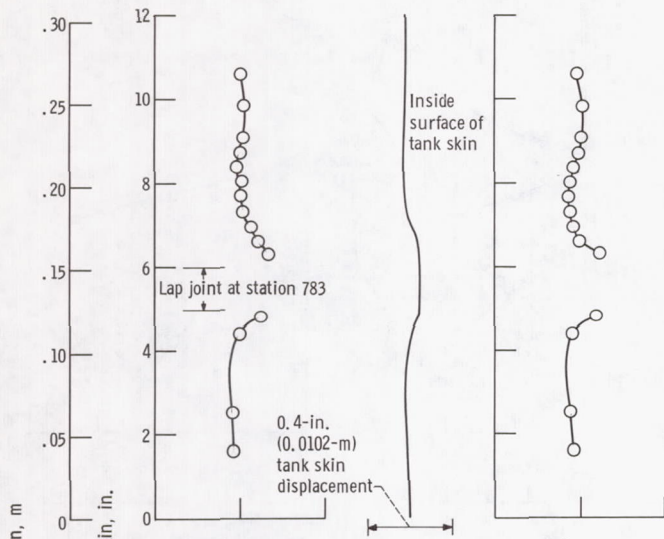
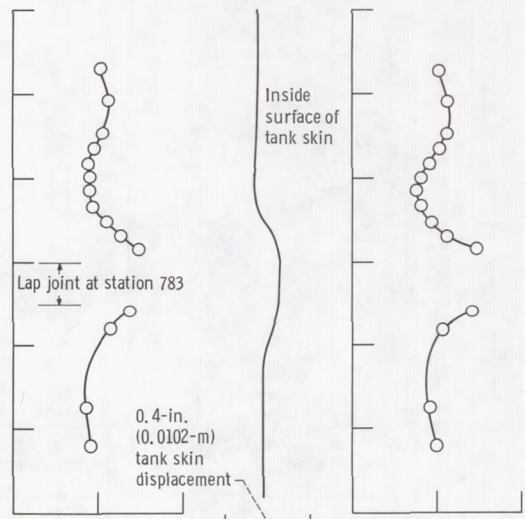


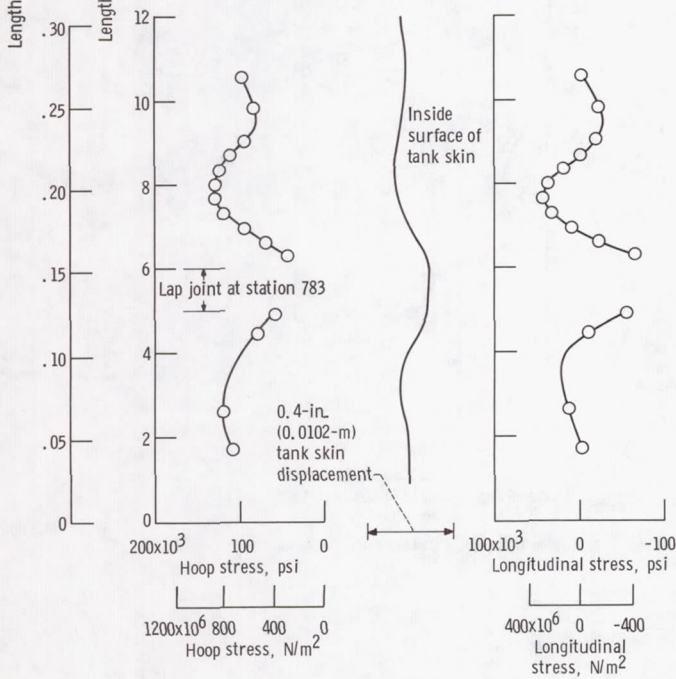
Figure 22. - Continued.



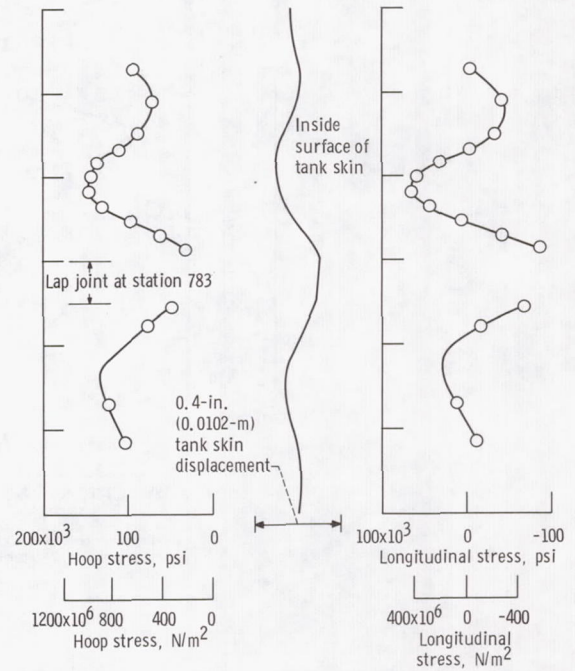
(i) Bending moment,  $6.34 \times 10^6$  inch-pounds ( $0.715 \times 10^6$  m-N); axial load, 75 800 pounds (336 000 N); ullage pressure, 24.0 psig ( $165\,200$  N/m<sup>2</sup>).



(j) Bending moment,  $7.4 \times 10^6$  inch-pounds ( $0.835 \times 10^6$  m-N); axial load, 75 800 pounds (336 000 N); ullage pressure, 24.0 psig ( $165\,200$  N/m<sup>2</sup>).

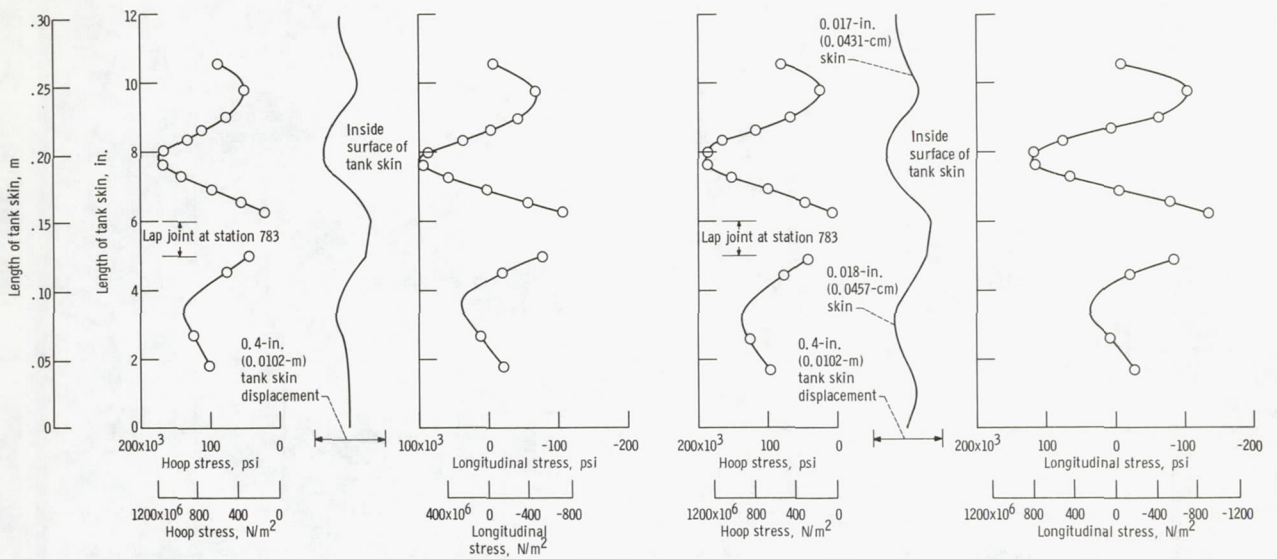


(k) Bending moment,  $7.95 \times 10^6$  inch-pounds ( $0.897 \times 10^6$  m-N); axial load, 75 800 pounds (336 000 N); ullage pressure, 24.0 psig ( $165\,200$  N/m<sup>2</sup>).



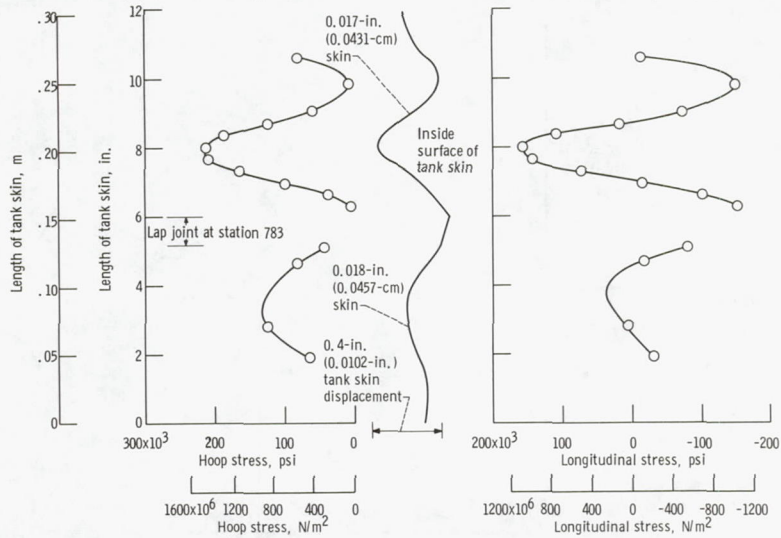
(l) Bending moment,  $8.5 \times 10^6$  inch-pounds ( $0.96 \times 10^6$  m-N); axial load, 75 800 pounds (336 000 N); ullage pressure, 24.0 psig ( $165\,200$  N/m<sup>2</sup>).

Figure 22. - Continued.



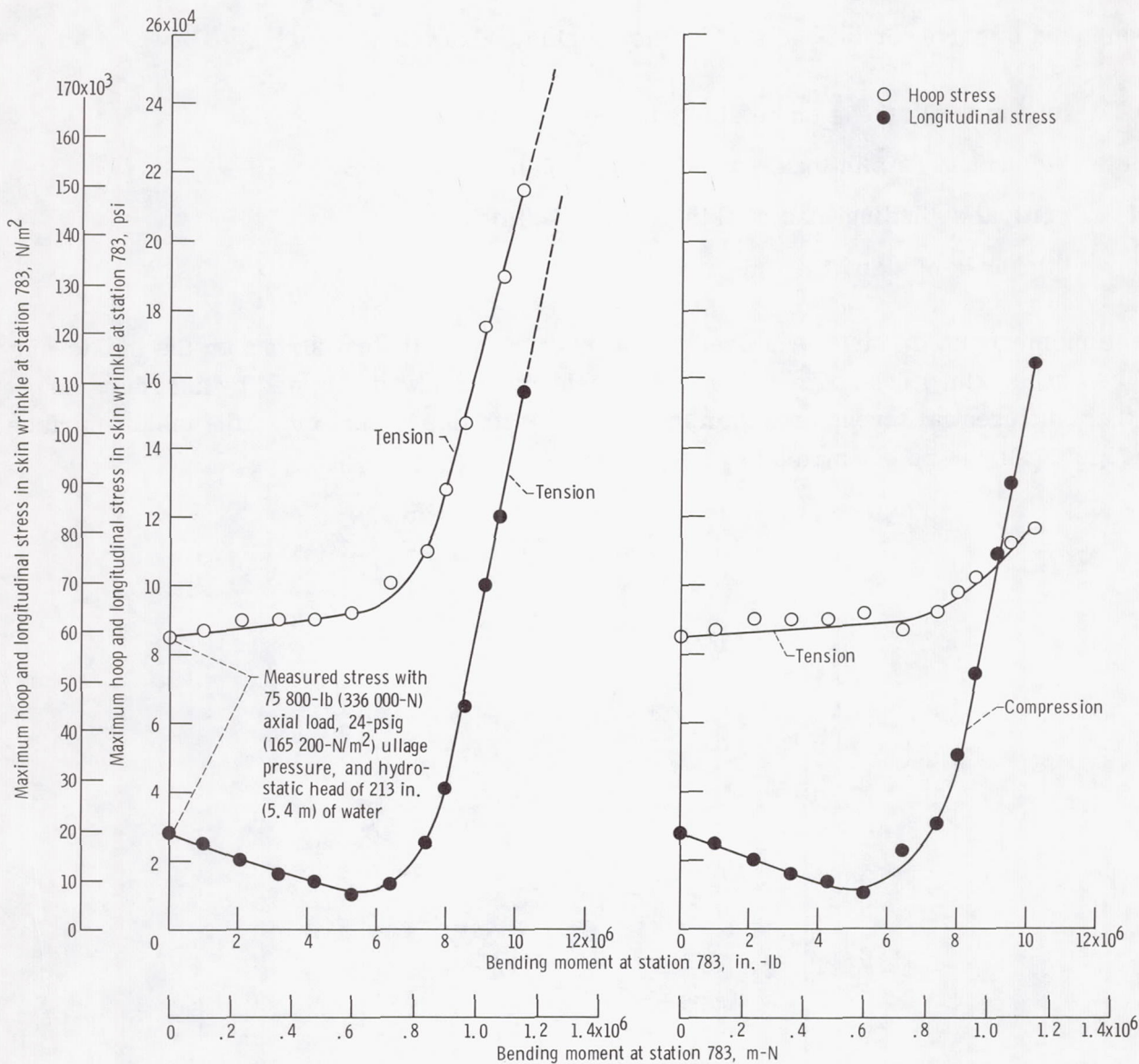
(m) Bending moment,  $9.06 \times 10^6$  inch-pounds ( $1.025 \times 10^6$  m-N); axial load, 75 800 pounds (336 000 N); ullage pressure, 24.0 psig (165 000 N/m<sup>2</sup>).

(n) Bending moment,  $9.6 \times 10^6$  inch-pounds ( $1.085 \times 10^6$  m-N); axial load, 75 800 pounds (336 000 N); ullage pressure, 24.0 psig (165 200 N/m<sup>2</sup>).



(o) Bending moment,  $10.17 \times 10^6$  inch-pounds ( $1.15 \times 10^6$  m-N); axial load, 75 800 pounds (336 000 N); ullage pressure, 24.0 psig (165 200 N/m<sup>2</sup>).

Figure 22. - Concluded.



(a) Maximum hoop and longitudinal stress on outside surface of wrinkle at station 783.

(b) Maximum hoop and longitudinal stress on inside surface of buckle at station 783.

Figure 23. - Comparison of maximum stresses on inside and outside surfaces of tank skin with bending moment at station 783 (gages 1 to 8, fig. 12).

$$\sigma_{L, o} = \frac{N_c}{t} \pm \frac{6m}{t^2}$$

was used to solve for the moment in the wrinkle, where

- $\sigma_{L, o}$  longitudinal stress on outside surface, psi;  $N/m^2$
- $m$  moment in skin in local wrinkle, (in.-lb)/in.;  $(m-N)/m$
- $N_c$  critical wrinkling load of skin, lb/in.;  $N/m$
- $t$  thickness of skin, in.;  $m$

The moment  $m$ , in turn, was used to estimate the longitudinal stress on the inside surface of the skin. The hoop stress on the inside surface was obtained by assuming no strain differential through the skin thickness. With this assumption, the inside-surface hoop stress can be estimated by

$$\sigma_{H, i} = \sigma_{H, o} - 2\mu \left( \sigma_{L, o} + \frac{N_c}{t} \right)$$

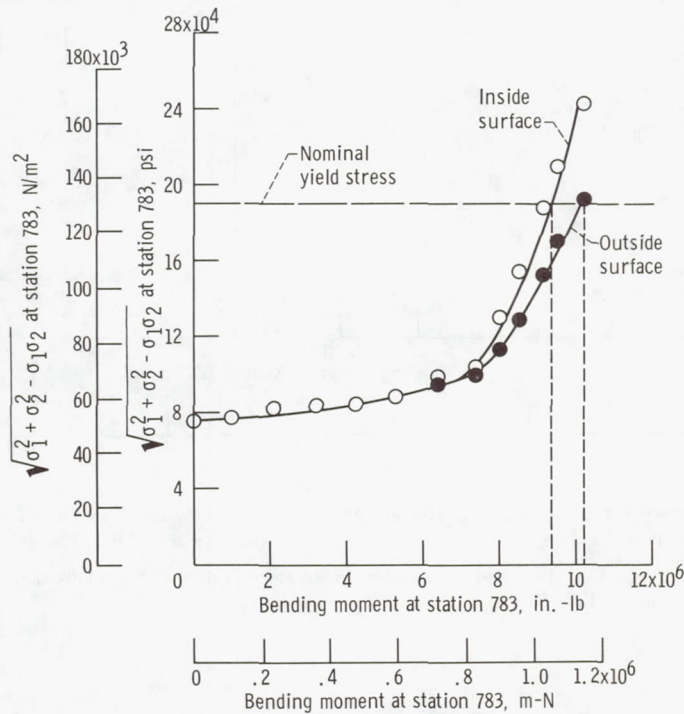


Figure 24. - Moment that produces yield in skin. Bending moment in Atlas as function of expression for failure from maximum distortion energy theory. Principal stresses,  $\sigma_1$  and  $\sigma_2$ , based on data presented in figure 23.

where

$\sigma_{H,o}$  outside-surface hoop stress, psi;  $N/m^2$

$\sigma_{L,i}$  inside-surface longitudinal stress, psi;  $N/m^2$

$\sigma_{H,i}$  inside-surface hoop stress, psi;  $N/m^2$

$\mu$  Poisson's ratio, in./in.; m/m

A derivation of the above equation is presented in appendix C.

From the stress in figures 23(a) and (b) the expression for yielding by the maximum distortion energy theory was used to obtain figure 24. This figure presents the expression for yield against applied moment. Figures 23(b) and 24 indicate yielding of the

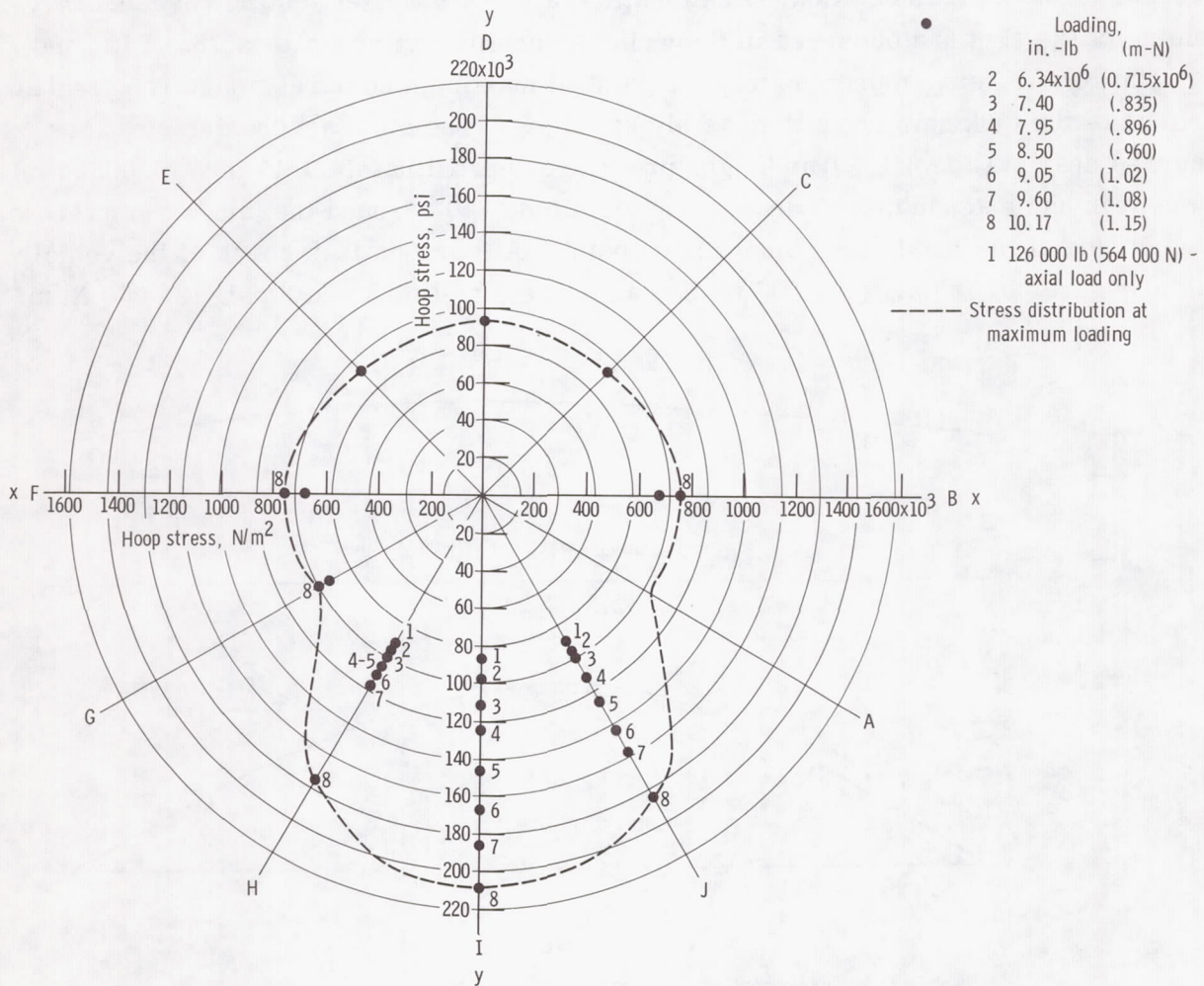


Figure 25. - Hoop stress distribution around Atlas circumference in plane of maximum wrinkle, station 780 (see fig. 11).

inner surface began at about  $9.4 \times 10^6$  inch-pounds ( $1.06 \times 10^6$  m-N) and on the outside surface at  $10.2 \times 10^6$  inch-pounds ( $1.15 \times 10^6$  m-N). In test 1, however, no visible sign of permanent set was evident after the application of  $10.2 \times 10^6$  inch-pounds ( $1.15 \times 10^6$  m-N) of moment.

Hoop stress distribution around the tank circumference in the plane of the deepest wrinkle in the station 783 area is presented in figure 25. The stress is plotted at each strain-gage location, identified by letters A to J which correlate with the gage orientation on the tank shown in figure 11. The stress at gage location H is questionable in that the gages were located near a vertical joint in the tank skin. The stiff vertical joint prevented the ideal wrinkling pattern of the skin from developing until the  $10.2 \times 10^6$ -inch-pound ( $1.15 \times 10^6$ -m-N) loading, at which time the vertical joint wrinkled and the stress assumed the more ideal symmetrical distribution.

At the conclusion of test 2 the deflection measurements returned to zero within the accuracy of the instrumentation. Examination of the Atlas after testing revealed that yielding of the skin had occurred in the wrinkles originating at stations 783, 812, and 841, station 812 being approximately the point of maximum compression. The yielded portions of the tank skin showed up as slight bulges. The most severe deformations occurred near station 812. The bulges protruded approximately 0.14 inch (0.00356 m) at the peak and extended, with decreasing amplitude,  $70^\circ$  around the tank circumference on each side of the maximum compression point. A thorough leak check of the vehicle with pressures of 15 psig ( $103\,200$  N/m<sup>2</sup> gage) in the fuel tank and 8 psig ( $55\,000$  N/m<sup>2</sup>

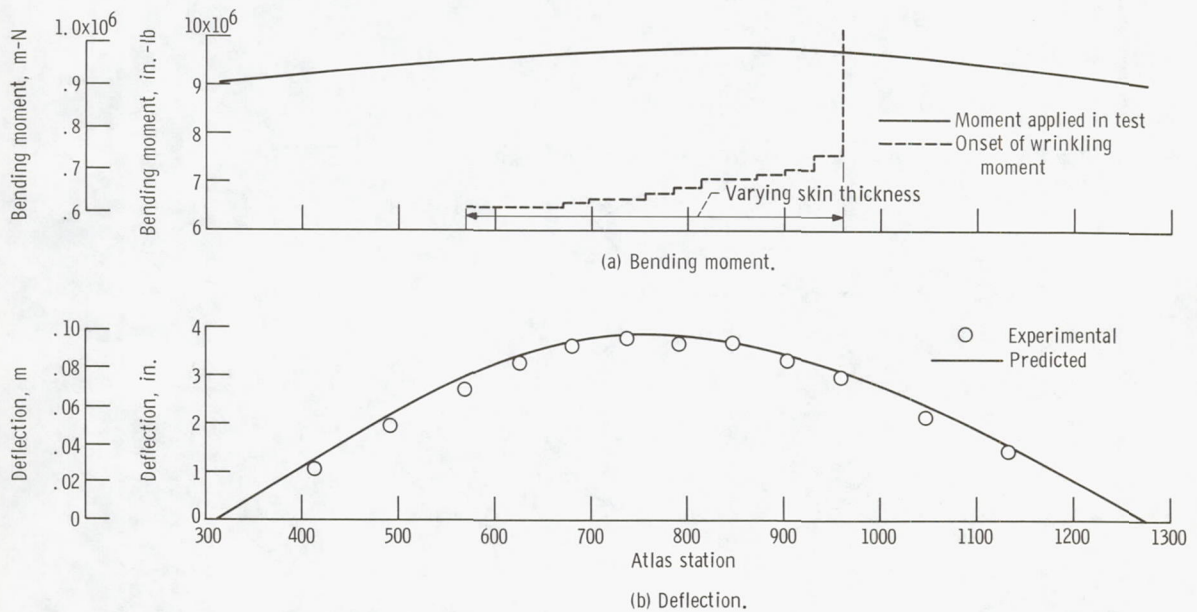


Figure 26. - Bending moment and deflection as function of Atlas station - test 3. Test conditions: axial load, 115 300 pounds (511 000 N); oxidizer tank pressure, 28.5 psig (196 000 N/m<sup>2</sup>); fuel tank pressure, 58.5 psig (403 000 N/m<sup>2</sup>); oxidizer tank filled with water to station 540; fuel tank filled with water to station 925.

gage) in the oxidizer tank, using soap solution, revealed no leaks in the tank structure.

For test 3, the vehicle was rotated  $40^{\circ}$ , moving the previously yielded skin away from maximum compression and placing the long (or B-1) pod in the position of the extreme compression fiber. Test 3 was devised to investigate the bending capability of the entire vehicle and not just the cylindrical monocoque portion of the tank as in tests 1 and 2. Test 3 placed a moment over the entire Atlas and interstage adapter in excess of  $9 \times 10^6$  inch-pounds ( $1.02 \times 10^6$  m-N), as shown in figure 26(a). The maximum load shown in figure 26 was limited by the capability of the test fixtures. This limited capability allowed an axial load of 115 300 pounds (512 000 N) instead of the 126 000 pounds (560 000 N) used for all other test 3 loadings. The measured deflection is compared to predicted deflection in figure 26(b) (see appendix A).

For typical flights at the time of maximum  $\alpha Q$ , the predicted bending moment distribution over the Atlas-Centaur vehicle indicates that the moments developed at stations 570 and 960 are approximately 80 percent of the peak moment at station 812. The moments applied to stations 570 and 960 in test 3 were 85 and 86 percent, respectively, of the maximum moment ( $11.2 \times 10^6$  in.-lb, or  $1.265 \times 10^6$  m-N) established in test 2 for station 812. Therefore, these test loadings show that the overall bending-strength envelope of the Atlas is compatible with the capability of the center portion (approx. station 783) of the oxidizer tank for typical Atlas-Centaur launches.

Figure 27 shows the load distribution around the tank circumference in the middle of the 0.014-inch- (0.000356-m-) thick skin just below station 570 during test 3. The curves show predicted longitudinal load against tank circumference compared with strain-gage test data. The element of the tank circumference at the  $270^{\circ}$  point received maximum compression. As the moment increased from  $6.3 \times 10^6$  to  $6.9 \times 10^6$  inch-pounds ( $0.71 \times 10^6$  to  $0.78 \times 10^6$  m-N), wrinkling of the skin began, as indicated by the flat portion of each load curve in figure 27. The length of the flat portion describes the extent of wrinkling around the circumference. The curves indicate that the wrinkle angle progresses from about  $52^{\circ}$  at  $6.9 \times 10^6$  inch-pounds ( $0.78 \times 10^6$  m-N) to  $152^{\circ}$  at  $9.6 \times 10^6$  inch-pounds ( $1.085 \times 10^6$  m-N). These strain-gage data, in general, agree with the predictions and confirm the similar data evaluated in test 1 (fig. 16). The loading of test 3 placed a maximum tensile load of 1534 pounds per inch (268 000 N/m) and a maximum compressive load of 910 pounds per inch (159 000 N/m) on the ring at station 570. At the conclusion of test 3, close visual inspection of the test vehicle revealed no evidence of yielding or damage to the tank skins, the ring at station 570, the area around station 960 (intermediate bulkhead junction), or the interstage adapter. A soapbubble check at

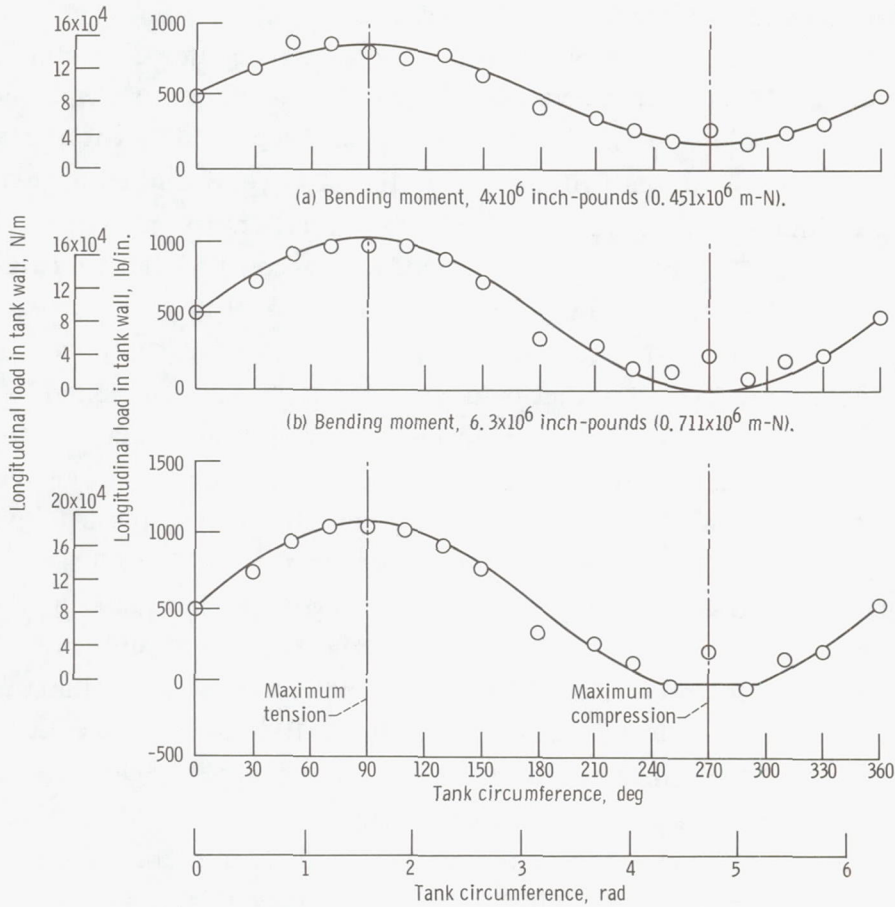
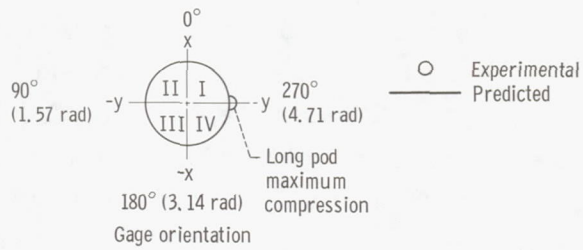
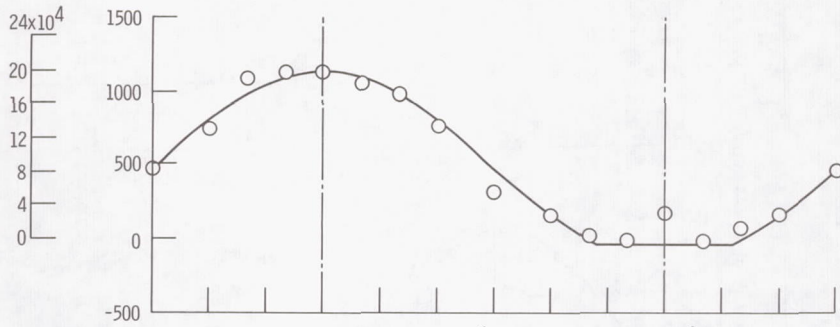
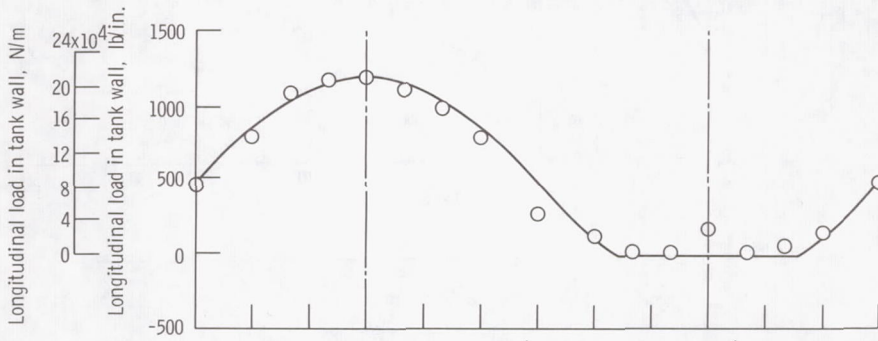


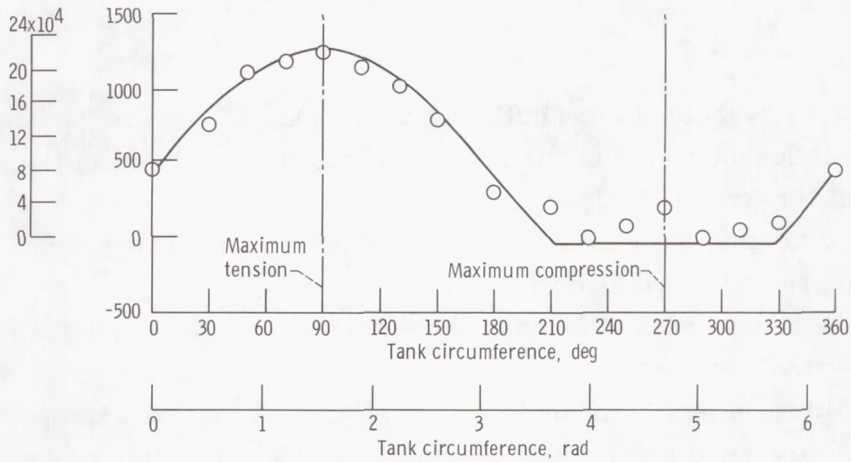
Figure 27. - Measured load distribution around circumference of Atlas at station 584 compared with predicted - test 3. (Flat portion of curves indicates portion of tank skin that has wrinkled.)



(d) Bending moment,  $7.4 \times 10^6$  inch-pounds ( $0.835 \times 10^6$  m-N).



(e) Bending moment,  $7.9 \times 10^6$  inch-pounds ( $0.891 \times 10^6$  m-N).



(f) Bending moment,  $8.5 \times 10^6$  inch-pounds ( $0.96 \times 10^6$  m-N).

Figure 27. - Continued.

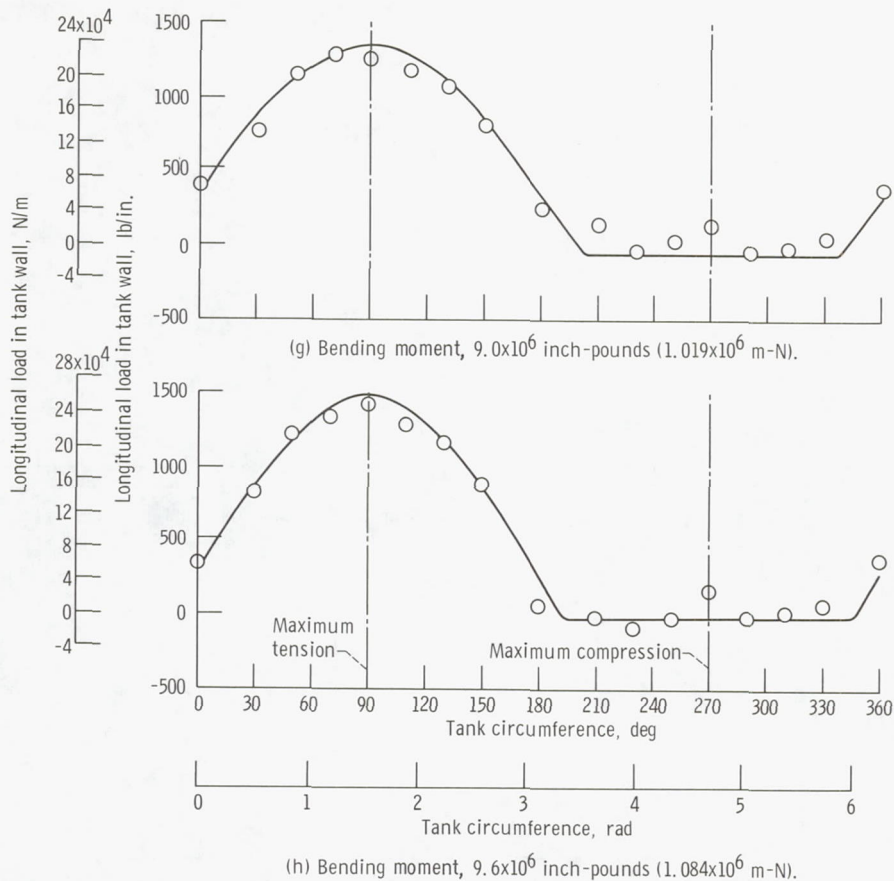


Figure 27. - Concluded.

standby pressures revealed no indication of tank leakage. Figure 28 depicts the Atlas tank under the influence of the maximum test 3 load that is shown in figure 26. The pod in the right foreground of figure 28 is receiving maximum compression. Wrinkles can be observed at each lap joint in the oxidizer tank. The severe wrinkles at station 812 are in the skin previously yielded in test 2.

Through the course of the series of three tests, the middle portion of the Atlas oxidizer tank went in and out of wrinkling eight times. Wrinkling loads were applied and removed four times in test 3, involving sections of tank skin that had previously been stressed beyond the yield point. The previously yielded condition of several tank skins, which resulted from test 2, appeared to have little effect on either the ability of the tank to sustain wrinkling loads or the predictability of the tank behavior. Figure 29 summarizes the maximum moment loadings applied to the vehicle in the test series.

Skin wrinkling that occurred near, or under, attachments to the tank wall, such as the equipment pods, appeared to have no adverse effect on the structural integrity of either the tank skin or the attachment brackets. An example of wrinkling under brackets

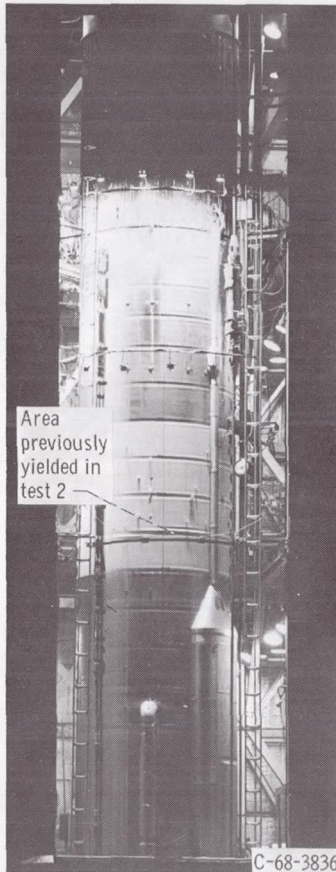


Figure 28. - Typical wrinkle pattern - test 3.

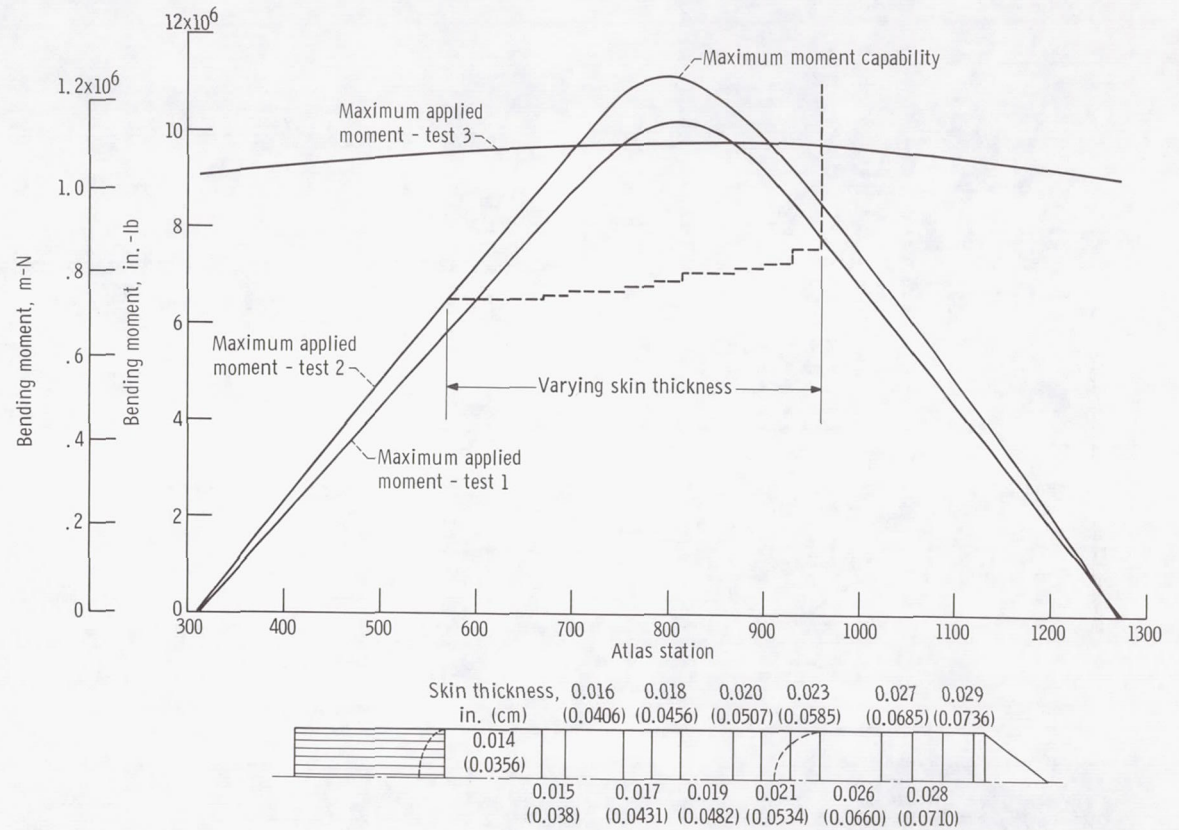
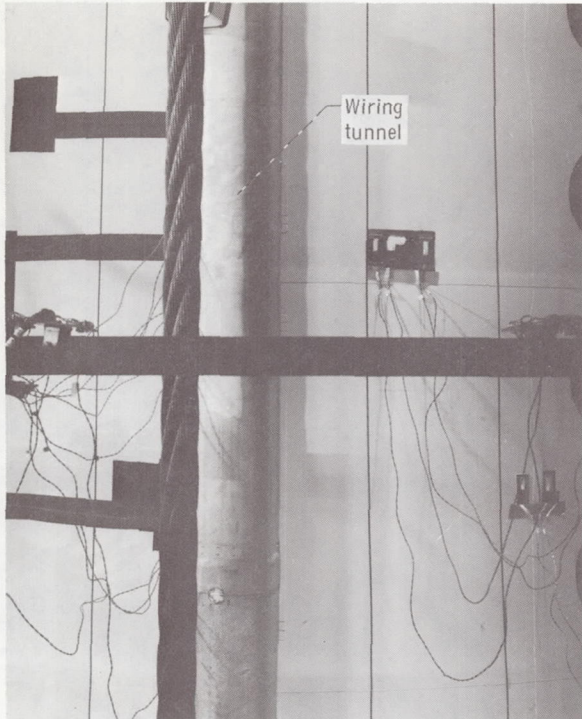
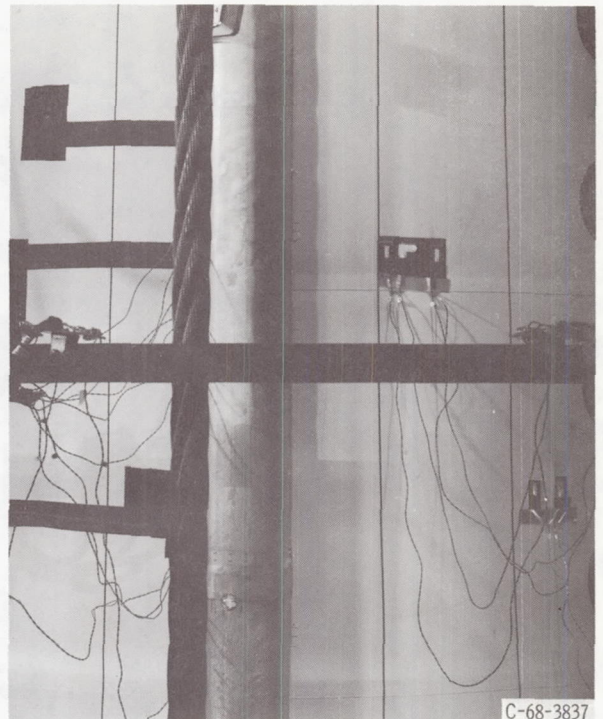


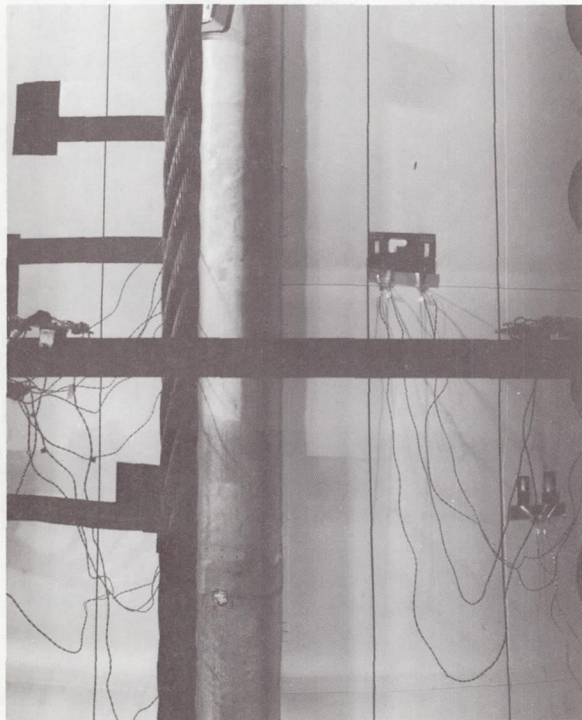
Figure 29. - Maximum applied moment as function of Atlas station.



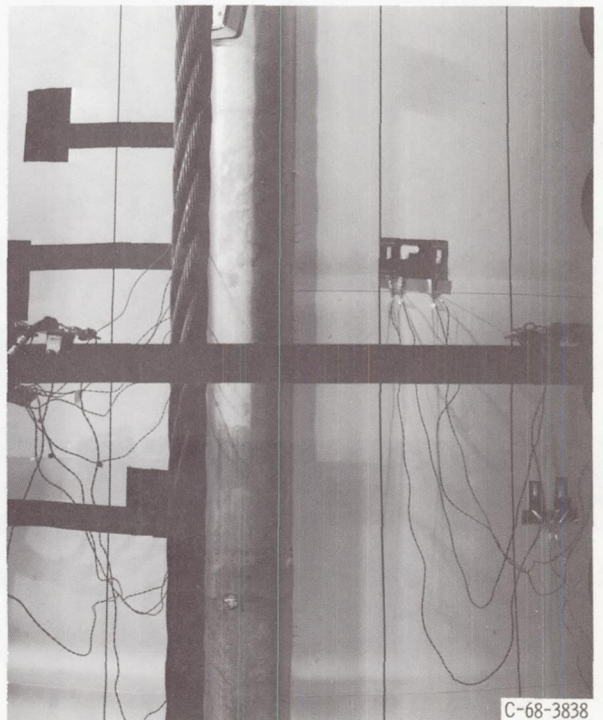
(a) Bending moment,  $6.35 \times 10^6$  inch-pounds ( $0.716 \times 10^6$  m-N).



(b) Bending moment,  $7.4 \times 10^6$  inch-pounds ( $0.835 \times 10^6$  m-N).

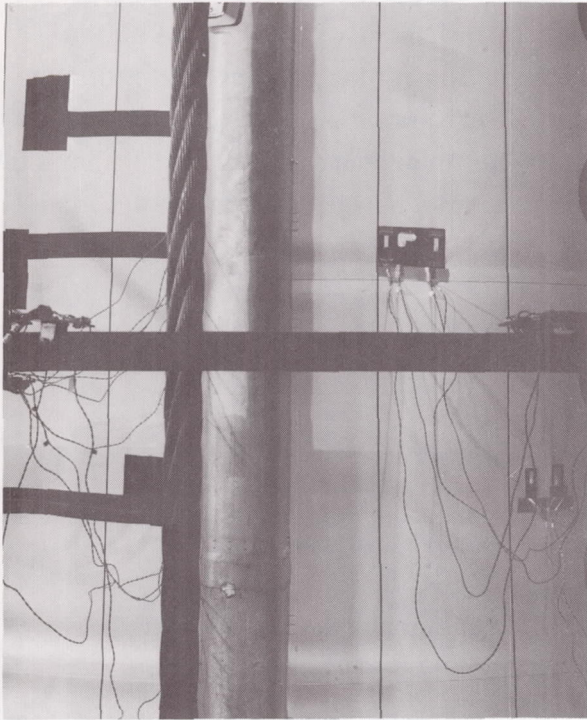


(c) Bending moment,  $7.95 \times 10^6$  inch-pounds ( $0.898 \times 10^6$  m-N).

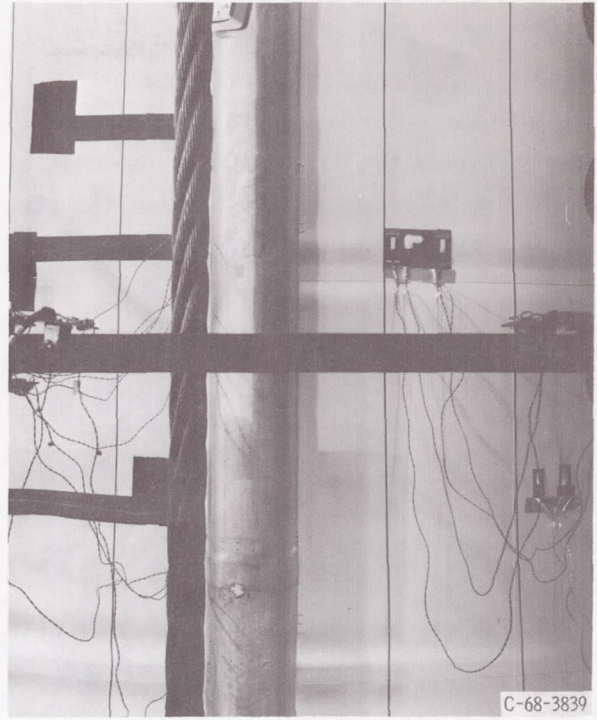


(d) Bending moment,  $8.50 \times 10^6$  inch-pounds ( $0.96 \times 10^6$  m-N).

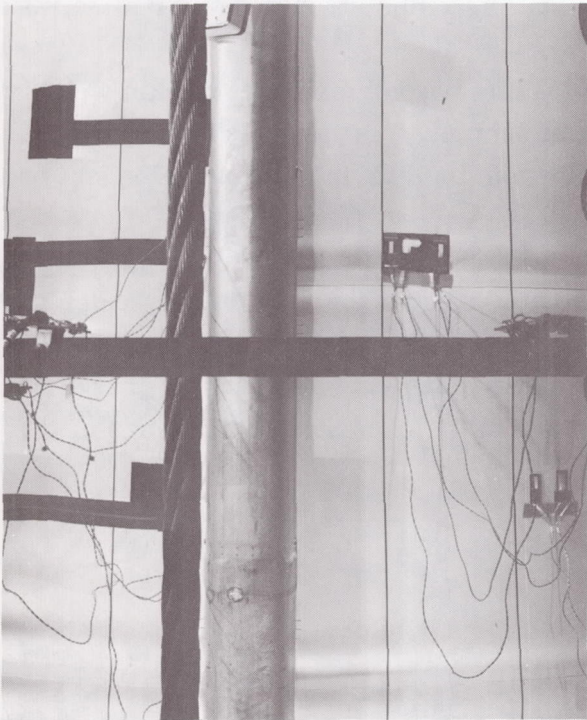
Figure 30. - Wrinkling under wiring tunnel - test 3.



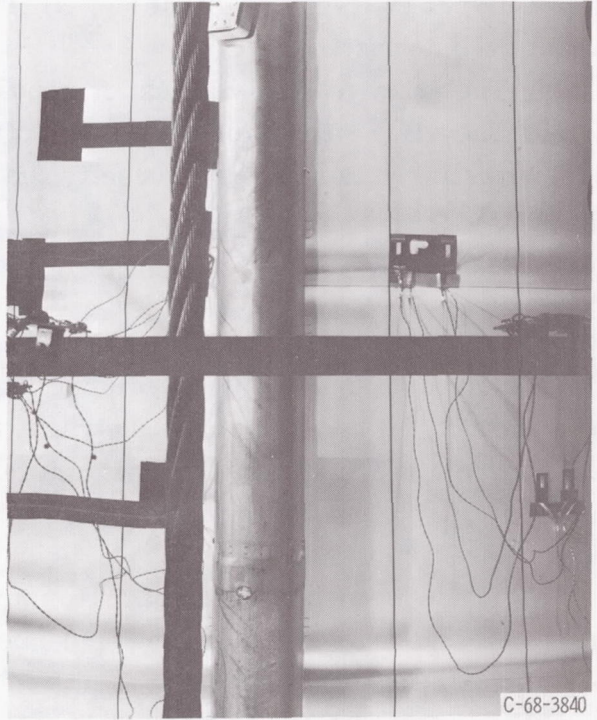
(e) Bending moment,  $9.05 \times 10^6$  inch-pounds ( $1.023 \times 10^6$  m-N).



(f) Bending moment,  $9.6 \times 10^6$  inch-pounds ( $1.85 \times 10^6$  m-N).



(g) Bending moment,  $10.15 \times 10^6$  inch-pounds ( $1.15 \times 10^6$  m-N).



(h) Bending moment,  $10.9 \times 10^6$  inch-pounds ( $1.23 \times 10^6$  m-N).

Figure 30. - Concluded.

is shown in figure 30. The reinforcing or stiffening effect of the longitudinal seams in the skins did disturb the predicted wrinkle pattern in the heavily loaded area at station 812. The vertical stiffener created by the longitudinal joint precipitated a discontinuity in the wrinkles as they progressed around the circumference of the tank. This deviation from the predicted behavior is evident in the foreground of figure 28 where the deep wrinkle at station 812 terminated above the circumferential lap joint at the longitudinal joint and shifted down below the lap joint to the less stiff portion of the tank.

## CONCLUDING REMARKS

The results of this series of tests of the Atlas booster can be summarized as follows:

1. Postwrinkling behavior as predicted by reference 1 and experienced on small-scale model tests, in general, is valid for full-scale Atlas tanks.
2. Under the conditions of this investigation, the moment capability of the pure monocoque portion of the Atlas oxidizer tank is at least  $11.2 \times 10^6$  inch-pounds ( $1.265 \times 10^6$  m-N).
3. Under the conditions of these tests, the Atlas vehicle can sustain moments of at least  $9 \times 10^6$  inch-pounds ( $1.02 \times 10^6$  m-N) at any station on the structure and maintain structural integrity.
4. The Atlas vehicle will sustain repeated loading beyond the onset of skin wrinkling.
5. The wiring tunnel and its method of attachment have a negligible effect on the skin-wrinkling pattern and conversely, the skin wrinkling has no detrimental effect on the tunnel.
6. Wrinkling of the tank wall initiates at the skin lap joints. However, the overall wrinkling behavior of the tank closely followed that predicted for a smooth cylinder without joints.

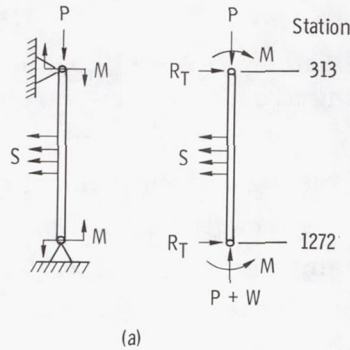
A method of analysis for predicting stress in the local wrinkle areas is presented in reference 11. A comparison of analytical results and the experimental findings of this test program is incorporated in that reference.

Lewis Research Center,  
National Aeronautics and Space Administration,  
Cleveland, Ohio, November 6, 1968,  
491-05-00-22.

## APPENDIX A

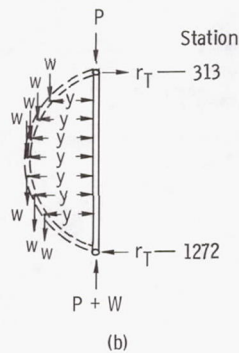
### METHOD OF PREDICTING BEAM DEFLECTIONS

The following procedure for obtaining the predicted deflection of the Atlas beam was established for the Plum Brook tests. The Atlas was considered as a pin-supported beam column, idealized as shown in sketch a where  $P$  is the applied axial load,  $R_T$



is the reaction to the tower,  $M$  is the applied moment couple,  $S$  is the applied shear load, and  $W$  is the vehicle weight.

For tests 1 and 2 the applied moments  $M$  were zero. For test 3 the applied shear loads  $S$  were zero. As the shear  $S$  or moment  $M$  is applied, the beam deflects. These deflections induce additional moments (secondary moments) through the action of the applied axial load  $P$  and the vehicle weight  $W$ . The secondary moments were obtained as indicated in sketch b where  $y$  is the deflection induced by applied shear  $S$  or moment  $M$ ,  $w$  indicates points where vehicle weight is considered to be concentrated,  $r_T$  is the reaction to the tower induced by deflections,  $P$  is the axial load, and  $W$  is the vehicle weight.



The conjugate beam method of calculating beam deflections was used to obtain the primary deflections represented as  $y$  in sketch b. With the column loaded as in sketch a, secondary moments were obtained at each  $w$  location by summing moments about each point, the moments being a function of  $P$ ,  $R_T$ , and  $W$ . The secondary moments thus obtained were added to the primary moments from the applied loads, and the beam deflections were recalculated with the conjugate beam concept, by using this total moment distribution. The deflections presented in this report were obtained with iterations of this procedure.

Before wrinkling of the tank skin the deflection is linear with load. After the onset of wrinkling the deflection becomes nonlinear. In the nonlinear region the stiffness is obtained by using an effective moment of inertia  $I_{\text{eff}}$ , ( $I_{\text{eff}} = tR^3 [\theta - \sin \theta \cos \theta]$ ) that is a function of the extent of wrinkling around the tank circumference. The origin of  $I_{\text{eff}}$  is presented in appendix B.

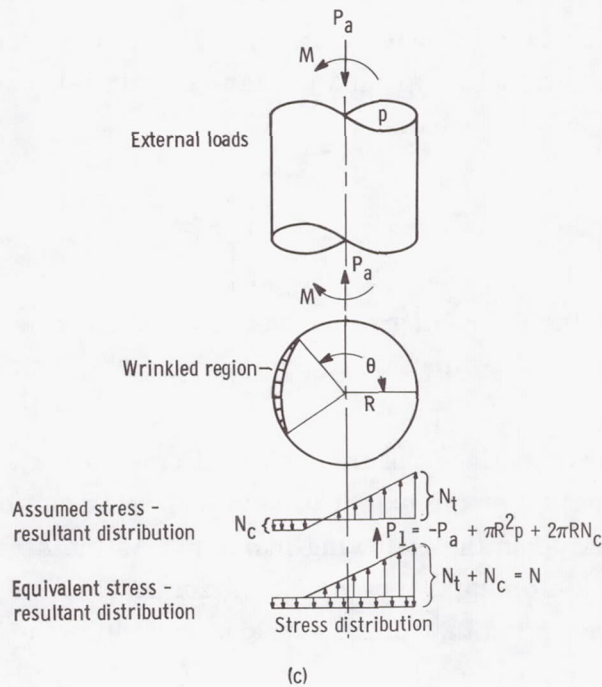
To monitor the magnitude of the secondary moment during testing, a ratio of secondary moment to deflection was established with the above procedure. With the assumption that the secondary moment remains proportional to deflection, this ratio was used with the deflections measured during testing to determine the total bending moment on the vehicle at any time in the loading sequence.

## APPENDIX B

### BEAM ANALOGY EQUATIONS FOR POSTWRINKLING STRENGTH

A relatively simple analysis was used for predicting the strength of the Atlas test vehicle. The analysis outlined herein is presented in greater detail in reference 1.

The bending stress distribution is assumed to be linear with the applied bending moment in the unwrinkled region and constant in the wrinkled region. The pressurized cylinder (sketch c) resists an external axial load  $P_a$  and an external bending moment



M. The bending moment is resisted by the load varying from zero at angle  $\theta$  to a maximum of  $N$  per unit length. The pressure, axial load, and uniform critical wrinkling load  $N_c$  have no bending moment about the longitudinal centerline. Integrating the values for the triangular distribution yields the following equation:

$$P_1 = \frac{2NR(\sin \theta - \theta \cos \theta)}{1 - \cos \theta} \quad (1)$$

Summing the bending moment of the  $N$  distribution about the cylinder centerline gives

$$M = \frac{NR^2(\theta - \sin \theta \cos \theta)}{1 - \cos \theta} \quad (2)$$

The critical wrinkling load  $N_c$  for the various skin thicknesses is obtained with the general equation

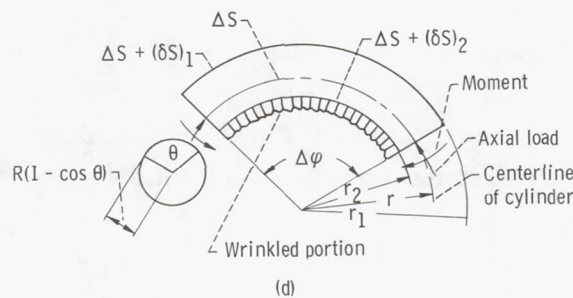
$$N_c = \frac{1}{\sqrt{3(1 - \mu^2)}} \left( \frac{Et^2}{R} \right) \quad (3)$$

for a thin-walled unpressurized cylinder (ref. 3). These equations can be used to determine the stress or load distribution around the tank circumference. The total axial tensile force  $P_1$  can also be expressed as

$$P_1 = -P_a + \pi R^2 p + 2\pi R N_c \quad (4)$$

With this expression and the preceding equations, the extent of wrinkling around the tank circumference can be found as a function of applied moment, axial load, and internal ullage pressure.

To define the nonlinear stiffness of the wrinkled tank, an effective moment of inertia  $I_{\text{eff}}$  that is a function of the extent of skin wrinkling can be used. This effective moment of inertia is derived in the following manner. As the stress  $N_t$  varies in a distance  $R(1 - \cos \theta)$ , an elemental length of cylinder  $\Delta S$  bends through an angle  $\Delta \varphi$  (sketch d). With the assumption that plane sections remain plane, these equations can be obtained from sketch d.



$$\Delta S + (\delta S)_1 = r_1 \Delta \varphi \quad (5a)$$

$$\Delta S + (\delta S)_2 = r_2 \Delta \varphi \quad (5b)$$

$$r_1 - r_2 = R(1 - \cos \theta)$$

Thus,

$$r_1 = R(1 - \cos \theta) + \frac{\Delta S + (\delta S)_2}{\Delta \varphi}$$

and

$$\Delta S + (\delta S)_1 = \Delta \varphi R(1 - \cos \theta) + \Delta S + (\delta S)_2$$

giving

$$\Delta \varphi = \frac{(\delta S)_1 - (\delta S)_2}{R(1 - \cos \theta)} \quad (6)$$

Since  $\epsilon_1 = N_t/Et$  and  $\epsilon_2 = N_c/Et$

$$(\delta S)_1 - (\delta S)_2 = \epsilon_1 \Delta S - \epsilon_2 \Delta S$$

or

$$(\delta S)_1 - (\delta S)_2 = \frac{\Delta S}{Et} (N_t + N_c) \quad (7)$$

Now, substituting equation (7) into equation (6) yields

$$\Delta \varphi = \Delta S \frac{N_t + N_c}{EtR(1 - \cos \theta)}$$

or

$$\frac{\Delta \varphi}{\Delta S} = \frac{N_t + N_c}{EtR(1 - \cos \theta)} \quad (8)$$

$$\frac{\Delta\varphi}{\Delta S} = \frac{M}{EI_{\text{eff}}} \quad (9)$$

(ref. 12) where  $I_{\text{eff}}$  is the effective moment of inertia. Substituting equation (8) into equation (9) and adjusting terms give

$$I_{\text{eff}} = \frac{MtR(1 - \cos \theta)}{N_t + N_c} \quad (10)$$

Now substituting equation (2) into equation (10) and noting  $N_t + N_c = N$  gives

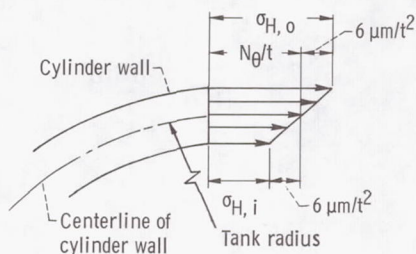
$$I_{\text{eff}} = tR^3(\theta - \sin \theta \cos \theta) \quad (11)$$

This expression for moment of inertia can be used for deflection computations of pressure stabilized vehicles in the nonlinear (wrinkled) range.

## APPENDIX C

### DERIVATION OF EQUATION FOR INSIDE-SURFACE HOOP STRESS

The origin of the equation  $\sigma_{H,i} = \sigma_{H,o} - 2\mu(\sigma_{L,o} + N_c/t)$  for hoop stress inside the tank is illustrated with the following sketch (tension considered positive):



where

- $\sigma_{H,i}$     inside-surface hoop stress, psi;  $N/m^2$
- $\sigma_{H,o}$     outside-surface hoop stress, psi;  $N/m^2$
- $\sigma_{L,i}$     inside-surface longitudinal or bending stress, psi;  $N/m^2$
- $\sigma_{L,o}$     outside-surface longitudinal or bending stress, psi;  $N/m^2$
- $N_\theta$       tensile hoop load in skin from internal pressure, lb/in.;  $N/m$
- $m$         bending moment in wrinkle, (in. -lb)/in.;  $(m-N)/m$
- $\mu$         Poisson's ratio, in. /in.;  $m/m$
- $t$         skin thickness, in.;  $m$
- $N_c$       critical wrinkling load for skin, in. -lb;  $(m-N)$

The principal stresses can be expressed as

$$\sigma_{L,i} = -\frac{6m}{t^2} - \frac{N_c}{t}$$

$$\sigma_{L,o} = \frac{6m}{t^2} - \frac{N_c}{t}$$

$$\sigma_{H, i} = \frac{N_{\theta}}{t} - \frac{\mu 6m}{t^2}$$

$$\sigma_{H, o} = \frac{N_{\theta}}{t} + \frac{\mu 6m}{t^2}$$

Values of  $\sigma_{H, o}$  and  $\sigma_{L, o}$  were obtained with strain gages and used to obtain  $N_{\theta}/t$  as follows:

$$\frac{N_{\theta}}{t} = \sigma_{H, o} - \frac{\mu 6m}{t^2}$$

but

$$\sigma_{L, o} = \frac{6m}{t^2} - \frac{N_c}{t}$$

Therefore,

$$\frac{N_{\theta}}{t} = \sigma_{H, o} - \mu \left( \sigma_{L, o} + \frac{N_c}{t} \right)$$

Thus,

$$\begin{aligned} \sigma_{H, i} &= \frac{N_{\theta}}{t} - \mu \left( \sigma_{L, o} + \frac{N_c}{t} \right) \\ &= \sigma_{H, o} - \mu \left( \sigma_{L, o} + \frac{N_c}{t} \right) - \mu \left( \sigma_{L, o} + \frac{N_c}{t} \right) \\ &= \sigma_{H, o} - 2\mu \left( \sigma_{L, o} + \frac{N_c}{t} \right) \end{aligned}$$

## REFERENCES

1. Peery, David J.: Post-Buckling Strength of a Pressurized Cylinder. Rep. GD/A-DDG-64-024A, General Dynamics/Astronautics (NASA CR-54802), Oct. 16, 1964.
2. Jahsman, W. E.: Combined Bending and Compression of a Pressurized Circular Cylindrical Membrane Column. *J. Eng. Industry*, vol. 87, no. 3, Aug. 1965, pp. 372-378.
3. Weingarten, V.: Effects of Internal Pressure on the Buckling of Circular Cylindrical Shells Under Bending. Rep. STL 7102-0033-RU-000, EM 11-12, Space Technology Labs., TRW, Inc., 1961.
4. Anon.: Buckling of Thin-Walled Circular Cylinders. NASA SP-8007, 1965.
5. McComb, Harvey G., Jr.; Zender, George W.; and Mikulas, Martin M., Jr.: The Membrane Approach to Bending Instability of Pressurized Cylindrical Shells. Collected Papers on Instability of Shell Structures. NASA TN D-1510, 1962, pp. 229-237.
6. Seide, P.; Weingarten, V. I.; and Morgan, E. J.: Development of Design Criteria for Elastic Stability of Thin Shell Structures. Rep. STL/TR-60-0000-19424, Space Technology Labs., TRW, Inc., 1960.
7. Suer, Herbert S.; Harris, Leonard A.; Skene, William T.; and Benjamin, Roland J.: The Bending Stability of Thin-Walled Unstiffened Circular Cylinders Including Effects of Internal Pressure. *J. Aeron. Sci.*, vol. 25, no. 5, May 1958, pp. 281-287.
8. Leaumont, Walter J., Jr.: Collapse Tests of Pressurized Membrane-like Circular Cylinders for Combined Compression and Bending. NASA TN D-2814, 1965.
9. Zender, George W.: The Bending Strength of Pressurized Cylinders. *J. Aerospace Sci.*, vol. 29, no. 3, Mar. 1962, pp. 362-363.
10. Miller, Robert P.; and Gerus, Theodore: Bending Strength of a Large Thin-Walled Pressure-Stabilized Cylinder Beyond Onset of Compressive Skin Wrinkling. NASA TM X-1311, 1966.
11. Greenbaum, G. A.; and Conroy, D. C.: Post-Wrinkling Analysis of Highly Pressurized Cylindrical and Conical Shells of Revolution Subjected to Bending Loads. Vol. I and II. TRW, Inc., Oct. 15, 1967.
12. Shanley, F. R.: *Strength of Materials*. McGraw-Hill Book Co., Inc., 1957.

